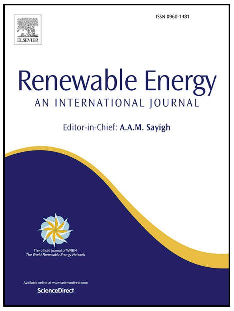

Wave climate and energy resources in the Mariana Islands from a 42-year high-resolution hindcast

Ning Li, Gabriel García Medina, Zhaoqing Yang, Kwok Fai Cheung, David Hitzl, Yi-Leng Chen

PII: S0960-1481(23)00725-5

DOI: https://doi.org/10.1016/j.renene.2023.05.093

Reference: RENE 18835

To appear in: *Renewable Energy*

Received Date: 9 December 2022

Revised Date: 8 May 2023

Accepted Date: 22 May 2023

Please cite this article as: Li N, García Medina G, Yang Z, Cheung KF, Hitzl D, Chen Y-L, Wave climate and energy resources in the Mariana Islands from a 42-year high-resolution hindcast, *Renewable Energy* (2023), doi: https://doi.org/10.1016/j.renene.2023.05.093.

CRediT author statement:

Ning Li: Conceptualization, Methodology, Investigation, Formal analysis, Data Processing Writing—original draft preparation, Writing—review and editing, Visualization.
Gabriel Garcia-Medina: Conceptualization, Methodology, Investigation, Formal analysis, Data Processing, Writing—review and editing, Visualization.
Zhaoqing Yang: Conceptualization, Methodology, Investigation, Resources, Writing—review and editing, Supervision, Project administration, Funding acquisition.
Kwok Fai Cheung: Conceptualization, Methodology, Writing—original draft preparation, Writing—review and editing, Supervision.
David Hitzl: Conceptualization, Writing—review and editing.
Yi-Leng Chen: Conceptualization, Writing—review and editing.

Wave climate and energy resources in the Mariana Islands from a 42-year high-resolution hindcast

Ning Li[1], Gabriel García Medina[2], Zhaoqing Yang[2,3]*, Kwok Fai Cheung[1], David Hitzl[4], Yi-Leng Chen[4]

[1] Department of Ocean and Resources Engineering, University of Hawaii at Manoa, HI 96822, USA

[2] Coastal Sciences Division, Pacific Northwest National Laboratory, Seattle, WA 98109, USA

[3] Department of Civil and Environmental Engineering, University of Washington, Seattle, WA, 98195, USA

[4] Department of Atmospheric Sciences, University of Hawaii at Manoa, HI 96822, USA

*Corresponding author: Zhaoqing.Yang@pnnl.gov

Wave climate and energy resources in the Mariana Islands from a 42-year high-resolution hindcast

Ning Li[1], Gabriel García Medina[2], Zhaoqing Yang[2,3]*, Kwok Fai Cheung[1], David Hitzl[4], Yi-Leng Chen[4]

[1] Department of Ocean and Resources Engineering, University of Hawaii at Manoa, HI 96822, USA

[2] Coastal Sciences Division, Pacific Northwest National Laboratory, Seattle, WA 98109, USA

[3] Department of Civil and Environmental Engineering, University of Washington, Seattle, WA, 98195, USA

[4] Department of Atmospheric Sciences, University of Hawaii at Manoa, HI 96822, USA

*Corresponding author: Zhaoqing.Yang@pnnl.gov

Abstract:

A high-resolution wave hindcast from 1979 to 2020 was developed for Guam and the Commonwealth of the Northern Mariana Islands, which are influenced by mesoscale and synoptic weather systems from the western Pacific Rim to the Central Pacific. The spectral wave modeling utilized structured global and unstructured regional grids with improved resolution in nearshore waters, where wave resources development is most feasible. The hindcast demonstrates its capability in capturing multi-modal seas through reproduction of bulk and partitioned wave parameters derived from altimetry and buoy measurements. The local wave climate is influenced by the year-round trade winds and tropical cyclones as well as seasonal monsoons, frontal systems, and mid-latitude high- and low-pressure systems. The strong intra-annual variation of the significant wave height and power flux reflects transitions between local and distant weather systems, which account for the diverse wave conditions comprised of short-period wind waves, intermediate-period seas, and long-period swells around the islands. Among the Pacific island regions, spectral partitioning is particularly important for describing the dominant wave components by period and direction with pertinent information for energy resources characterization and applications related to coastal engineering, ecosystem, and management in the Mariana Islands.

Keywords: Wave hindcast, Wave climate, Wave energy resources, Partitioned wave spectrum, Mariana Islands

1. Introduction

Most remote Pacific Island communities depend heavily on imported fossil fuels as an energy source, which is vulnerable to natural disasters and market volatility. A diversified energy portfolio including ocean wave resources is favorable for promoting energy independence in these isolated locations with proximity to the ocean. The Mariana Islands, located in the northwestern Pacific Ocean, are 2000 km from Japan, the Philippines, and New Guinea (Figure 1a). The island group includes Guam, an unincorporated territory of the US, as well as the most populous islands of the Commonwealth of the Northern Mariana Islands (CNMI) - Rota, Tinian, and Saipan. Although the islands are relatively small, their Exclusive Economic Zone (EEZ) covers a large region (970,772 km^2) with vast marine resources. On the inhabited islands, ocean waves play a significant role in coastal hazard management, coral reef ecology, and maritime activity all year round. To capture real-time wave conditions, a Waverider buoy was installed at 200 m depth off the east shore of Guam in 2003. Two additional wave buoys were deployed north of Guam at 500 m depth and north of Saipan at 487 m depth in 2012 (Figure 1b). The buoy records provide vital information for coastal activities but are insufficient to describe the complex wave climate due to sparse coverage, island blocking, limited years of record, and irregular downtimes. Numerical modeling, when appropriately validated, serves to extend the observation record by creating a synthetic time history, which can support wave energy resource quantification and coastal management activities.

Third-generation spectral wave models, such as WAVEWATCH III (Tolman and Chalikov, 1996; Tolman 2006, 2008, 2009) and WAM (WAMDIG 1988, Komen et al. 1994), have been utilized with coupled model systems including atmosphere, land, ocean, and sea ice components to produce wave hindcasts as part of global reanalysis products. The ERA-interim reanalysis produced by the European Centre for Medium-Range Weather Forecasts (ECMWF) includes wave data products from WAM for 1979 to 2019 at 1 arc-deg grid resolution (Dee et al., 2011). It was superseded by the recently released ERA5 reanalysis, which provides a global wave hindcast from 1950 to the present with 0.36 arc-degree resolution (Hersbach et al., 2020). The US National Centers for Environmental Prediction (NCEP) produced comparable datasets such as the Climate Forecast Reanalysis (CFSR) at 0.5 arc-deg resolution from 1979 to 2009 (Sara et al., 2010) and CFS version 2 (CFSv2) at 0.25 arc-deg resolution from 2010 onward (Saha et al., 2014). This facilitates development of global and regional wave hindcast at 0.5 arc-deg to 4 arc-min resolution using WAVEWATCH III (Chawla et al., 2012). The global hindcast datasets are suitable for wave climate and resources assessment at the basin level (Stopa and Cheung, 2014a, b), but do not have sufficient spatial resolution and provisions for shoaling and refraction in coastal waters around many of the Pacific islands including the Mariana Islands. In addition, shadowing around islands is a major local factor influencing available ocean wave resources in a multi-modal sea state (Stopa et al., 2011).

The Centre for Australian Weather and Climate Research (CAWCR) developed a 1979-2009 wave hindcast for the Central and South Pacific with resolution as fine as 4 arc-min in coastal waters (Durrant et al., 2019). The Changing Waves and Coasts of the

Pacific project utilized an earlier version of the CAWCR hindcast to assess the wave climate and seasonal variability for Guam (Durrant et al., 2014). The study focused on bulk parameters such as significant wave height and peak period derived from the combined sea state to provide a baseline assessment. Waves generated by local and distant weather systems, which have surface winds of varying strength and fetch, can have distinct heights, periods, and directions in the waters surrounding Guam (Bosserelle et al., 2014). To better understand the wave climate for Pacific islands such as Guam and the CNMI, an in-depth investigation of wave components within the mixed seas and their relationship with the near and far-field weather system is needed. The latest versions of spectral wave models such as WAVEWATCH III and SWAN, also known as Simulating WAves Nearshore (Booij et al., 1997; Booij et al., 1999), include a watershed algorithm (Hanson and Phillips, 2001) to partition the frequency-direction spectrum by dominant component. Wave parameters from the partitions can be used for separate analyses of wind waves and swells to better quantify global and regional wave resources (Arinaga and Cheung, 2012; Portilla-Yandún et al., 2015). The partitioned wave parameters have the advantage over the bulk parameters in providing detailed classification of energy resources by direction and frequency ranges (Ahn et al., 2022) and facilitate their statistical analyses for more accurate projection of extrema (Portilla-Yandún et al., 2020).

Under the US Department of Energy's nationwide Powering the Blue Economy initiative, the Pacific Northwest National Laboratory (PNNL) in collaboration with the University of Hawaii developed a high-resolution wave hindcast from 1979 to 2020 for characterization of energy resources around the US coastal regions and affiliated islands in the Pacific Ocean (García Medina et al., 2019, 2021; Yang et al., 2020). The modeled island regions include the EEZs around Hawaii, American Samoa, Baker and Howland Islands, the CNMI, Guam, Jarvis Island, Johnston Atoll, Palmyra Atoll, Kingman Reef, and Wake Island in the central and western Pacific as illustrated in

Figure 2. The use of unstructured computational grids in SWAN (Zijlema, 2010) is especially important for small islands by allowing a gradual, local refinement of the spatial representation for complex bathymetry and jagged shores. This provides a more accurate description of the wave shoaling, refraction, and dissipation in the nearshore region, where wave energy resources development is most feasible. The wave hindcasting follows the Technical Specification published by the International Electrotechnical Commission Technical Committee 114 (IEC-TC 114) to assure compatibility for resources assessment among oceanic and continental regions (García Medina et al., 2019, 2021; Yang et al 2018, 2019). Li et al. (2021) utilized the hindcast to study the wave climate in Hawaiian waters and complemented the IEC TS with the use of partitioned spectra to characterize wave resources in multimodal seas.

Located in the northwestern Pacific Ocean, the inhabited Mariana Islands are subject to waves influenced by ocean-surface winds originating from both Asia continental and Pacific oceanic weather systems with unique characteristics among other Pacific Island regions covered by the PNNL hindcast. Prior studies examined the local wave climate (Durrant et al., 2014; and Bosserelle et al., 2014), but additional work is still needed to explore its spatial-temporal relationship with weather systems and to quantify the multimodal seas by component for meaningful applications. In the present paper, we utilize the 42 years of high-resolution hindcast to investigate the weather patterns and wave climate characterizing the wave energy resources for Guam and the CNMI, while a companion paper in this special collection focuses on the PNNL hindcast around the Samoan Islands in the South Pacific Ocean (García Medina et al., 2023). Section 2 provides a summary of the hindcast model and data system from García Medina et al. (2021) followed by validation with satellite altimetry and buoy measurements around the Mariana Islands in Section 3. The validation includes an analysis of the spectral partitions at the buoys, delineating dominant components in the multimodal sea state for subsequent analyses. Section 4 links the representative wave patterns and weather systems to investigate the sources of the multimodal seas. This provides a framework to understand the composition and intra-annual variations of the hindcast significant wave height and energy flux in Section 5. The concluding remarks in section 6 includes key features of the wave climate, potential for wave energy development, and applications of the data products in the Mariana region.

2. Hindcast model and data system

The wave hindcast system is comprised of the third-generation spectral models WAVEWATCH III and SWAN with a suite of nested computational grids from the globe to the Mariana Islands (Figure 2). WAVEWATCH III covers the entire globe at 0.5 arc-deg, the central and western Pacific at 10 arc-min resolution, and the regions around the US and affiliated Pacific Island territories at 4 arc-min resolution. The three levels of model grids are two-way nested with direct information exchange during run time. The 4 arc-min regional grid, which extends about 1 arc-deg outside the EEZ of Guam and the CNMI, serves as a transition from the Pacific Island grid by producing two-dimensional spectral boundary conditions for the implementation of SWAN around the Mariana Islands. The SWAN grid is built on an unstructured triangular mesh with resolution refining from 5 km offshore to 100 m at the shore with less than 10% area change between adjacent elements for smooth transitions (Figure 3). The grid flexibility allows detailed local descriptions of the rugged shorelines, shallow shelves, harbors, and marinas extending the model validity into nearshore waters with optimal efficiency. Important coastal structures, not resolvable by the 100-m nearshore mesh, are manually incorporated for proper geospatial representation in the model.

Accurate wave modeling requires a digital elevation model (DEM) that can describe intricate seafloor features such as seamounts, shelves, channels, and nearshore reefs in shoaling waters. We compiled a DEM from high-resolution bathymetry and topography datasets for Guam and the CNMI with the Earth

Topography (ETOPO) Global Relief Model as the background. The datasets were obtained from multiple sources and rectified with the World Geodetic System 84 spheroid and the local mean sea level as the horizontal and vertical datums. They are listed in the order of precedence for computational grid generation:

- 2007 U.S. Army Corps of Engineers (USACE) LiDAR topography at 0.5 m resolution for the entire island of Guam.
- 2008 US Navy & National Oceanic and Atmospheric Administration (NOAA) multibeam bathymetry of Apra Harbor at 1 m resolution.
- 2001 USACE Scanning Hydrographic Operational Airborne (SHOALS) LiDAR bathymetry to 40 m depth at 4 m resolution.
- 2007 USACE LiDAR bathymetry at 4 m resolution (limited coverage).
- 2007 University of Hawaii School of Ocean and Earth Science and Technology (SOEST) multibeam bathymetry to 400 m depth at 5 m resolution.
- 2011 University of Hawaii SOEST multibeam bathymetry to 3.5 km depth at 60-m resolution.

The multibeam datasets are available from the Pacific Islands Benthic Habitat Mapping Center at the University of Hawaii (https://www.soest.hawaii.edu/pibhmc/cms/data-by-location/). The LiDAR datasets have recently been integrated into the Continuously Updated Digital Elevation Model (CUDEM) - 1/3 Arc-Second Resolution Bathymetric-Topographic Tiles (https://www.fisheries.noaa.gov/inport/item/48051).

The input forcing for wave hindcasting includes hourly surface winds with spatial resolutions of 0.5 arc-deg from CFSR for 1979-2020 and 0.25 arc-deg from CFSV2 for 2010- 2020. Orographic effects are not fully resolved in the wind field but are unlikely to influence the wave field due to the relatively small size of the Mariana Islands. The CFSR and CFSV2 winds are well reproduced over the ocean and proven accurate in wave modeling for other US regions (Allahdadi et al. 2019; Ahn et al. 2020; Garcia-Media et al. 2019, 2021a, 2021b; Yang et al. 2017, 2018, 2019, 2020; Wu et al. 2020).

The ST4 source term package developed by Arduin et al. (2010) is used in WAVEWATCH III and the spectrum is discretized into 24 direction bins following the setup of the NCEP global wave forecast (Chao et al., 2003a; Chao et al., 2003b) and 29 frequency bins with a logarithmic increment factor of 1.1 from 0.035 to 0.505 Hz. In SWAN, the default options for the source term, bottom friction, depth-induced breaking, and triad interactions are used. The SWAN spectrum is discretized with 5-deg directional bins and 31 logarithmically-spaced frequency bins from 0.035 to 0.505 Hz to account for energy density distributions. The higher directional resolution is needed to mitigate the garden sprinkler effects, which are amplified by refraction over the steep volcanic island slopes. The model configuration is consistent with the hindcast for the US West Coast, Alaska, and the Hawaiian Islands by following the IEC TS for wave resources characterization.

We implement the model system for wave hindcasting around the Mariana Islands for the period from 1979 to 2020. The 42-year hindcast dataset includes the bulk and partitioned wave parameters such as the significant wave height, peak period, and peak direction for all grid points within the SWAN domain as well as the frequency-direction spectra along the 100-m water depth contour, at distances 2 and 5 km from the shore, and at the three buoys near the islands. The computational time step is 2 min for a balance of accuracy and efficiency, while the output interval of 3 hours is sufficient to capture wave events from mesoscale weather phenomena. The dataset for the Mariana Islands along with those for other US and affiliated Pacific islands will be publicly available at the Registry of Open Data on AWS (Amazon Web Services) for implementation in coastal environment studies, wave climate analysis, and energy resources assessment.

3. Validation of wave hindcast

Satellite-borne altimeters have provided nearly continuous measurements covering most of the ocean since the GEOSAT (GEOdetic SATellite) mission in 1985. Despite the long orbital repeat cycle, the altimetry data serve as a valuable resource for model validation and assessment (e.g., Li et al., 2016; Stopa and Cheung, 2014; Dutheil et al., 2021). The Australian Ocean Data Network portal (https://portal.aodn.org.au/) provides the significant wave height derived from the Ku band measurements on multiple altimetry platforms (Ribal and Young, 2020). The dataset includes more than four million observations within the SWAN model domain from 1985 to 2020. We binned the dataset over a 0.2 arc-deg grid to allow for an adequate description of the spatial variation and provide sufficient data in each bin for statistical analysis. The data density in Figure 4a shows sufficient coverage with distinct tracks having more measurements. The hindcast significant wave height is interpolated to match the time and location of each available altimetry observation and bins with less than 200 data pairs are omitted in the computation of error metrics. Figures 4b, c, and d show the bias, linear correlation, and the root-mean-square-error (RMSE) of the hindcast against the altimetry data. Good agreement is indicated by a bias of less than 0.1 m as well as a correlation coefficient of over 0.9 and its relatively uniform distribution across the model region. The negative bias of the model results near Guam is consistent with experiences from local weather forecasters with the operational data products. The RMSE of 0.2~0.5 m is typical among hindcast datasets for other Pacific Island regions (Li et al., 2016, Durrant et al., 2014) and is not concerning given the similar range of errors in the altimetry-derived significant wave height (Yang and Zhang, 2019). The slightly higher RMSE to the north and west of the Mariana Islands is a result of the more dynamic weather systems around the western Pacific rim.

Wave buoy measurements are commonly considered as ground truth for the validation of model results. There are three Waverider buoys deployed, respectively, off the north shore of Saipan, and the north and east shores of Guam with Coastal Data

Information Program (CDIP) indexes 197, 196, and 121 (Figure 1b). The wave buoys continuously record sea-surface movement, from which the frequency-direction spectrum and parameters such as significant wave height, peak period, and peak direction are automatically derived every 30 minutes. Buoy 196 immediately north of Guam is the most exposed to the dominant wave components. The time series of the hindcast and recorded wave parameters from 2013 to 2020 are shown in Figure 5a and a close-up view of the comparison for 2017 in Figure 5b. The buoy records suggest a wide range of conditions with significant wave heights of 0.3-6.9 m, peak periods of 3.3-18.2 s, and directions typically from the southwest through east clockwise. The diverse waves have strong seasonal variations with large events above 4 m in the winter months and waves of 1-2 m in the summer months. The moderate summer sea state is occasionally interrupted by large waves from tropical cyclones passing nearby as indicated by rapid changes in wave directions from south to north. The hindcast follows the buoy measurements to capture both the seasonal variations and the individual wave events, despite slight overestimation of the small events and a tendency to underestimate the peak of some large events. The latter is likely due to limited resolution of strong winds near the core of large storms (Stopa and Cheung, 2014).

We pair the hindcast and buoy measurements of the same hour for a direct comparison. Figures 6a and 6b provide the scatter and Q-Q plots for the significant wave height from 2013 through 2020. The scatter plot gives a small RMSE of 0.3 m and a high correlation coefficient of 0.91 with 90% of the data pairs within ± 0.46 m of a perfect match. This point comparison corroborates the spatial comparison with altimetry data with an improved agreement and reiterates the good correspondence between the hindcast and observations. The large spreading for waves above 4 m may be attributed to timing differences of events between the two datasets. The quantile-quantile (Q-Q) plot eliminates any time difference to compare the statistical distributions. Despite the slight underestimation of the significant wave height in the range of 2 to 4 m, the hindcast is within 10% of the measurements even at the 99th and higher percentiles. Comparisons with available data at Buoys 121 and 197 show similar patterns (Figures A1-A4 in the appendix). The location of Buoy 121 on the east side of Guam is open to waves from the central Pacific that are partially blocked at Buoys 196 and 197. The recorded waves, which approach Guam from the east through the south in the summer, are complementary to the validation. Despite mismatching the peaks for some extreme events, the long-term hindcast provides a reliable dataset for statistical analysis and an accurate description of the overall sea state in the entire region.

The sea state comprises waves from multiple sources with distinct characteristics. Figure 7 illustrates the occurrence probability of the measured significant wave height and peak period at buoy #196 along with the distributions in the cardinal and ordinal directional sectors. Waves from the northeast are dominant 42% of the time, and these are followed by easterly and northerly waves with 24% and 18% occurrences. The remaining directional sectors account for less than 10% each. Waves from the southeast and south are rare and partially blocked by the island, and those that reach the buoy after wrapping around the headlands account for less than 0.2% of the time. Despite the disproportionate distribution among the directions, all show a dominant peak at 10 s and rapidly diminishing occurrence probability and significant wave height below 7 s. A second peak appears at 12 s from north and northwest with significant wave height ranges similar to those of the primary peak at 10 s. The results suggest a mix of dominant wave components in the Mariana Islands delineated by 7 and 11 s periods. Following the marine definitions of the US National Weather Service (https://www.weather.gov/gum/MarineDefinitions), we classify the multimodal seas into three main components identified as wind waves, seas, and swells for periods below 7s, of 7-11 s, and above 11 s, respectively. The classification of the dominant wave components is also consistent with local knowledge and the weather patterns in the Western and Central Pacific (Jordan, 1955; Lander 1994; Lander and Guard, 2003).

Since the wave climate analysis will be based on separate wave components from the hindcast, it is necessary to independently verify their delineation and to understand the model performance for each sea state.

For each component, we integrate the 2D spectrum from SWAN over the period range for the zeroth moment (m_0) and calculate the representative wave height $h_S = 4\sqrt{m_0}$ that reflects the energy level. Figure 8 shows good correspondence of the representative wave heights computed from the hindcast and records at #196 for 2017. The predefined period ranges capture distinct peaks of wind waves, seas, and swells, but are not absolute in delineating the wave components. There are some concurrent peaks between adjacent period ranges as the atmospheric forcing from weather systems is not always well distinguished from one another. The three components have distinct seasonal characteristics adding confidence to their delineation by period. The wind waves under 7 s are the most persistent with representative wave heights in the range of 0.5-2 m throughout the year. Seas of 7 to 11 s also have a year-round presence with higher energy in the winter than in summer. In particular, the representative wave height reaches 4 m in February and typically stays within 0.5~1.5 m from June to August. There is also a stronger correlation between the wind waves and seas in the winter months suggesting their generation from large weather systems with long fetches extending to the Mariana Islands. Swells with periods above 11 s are mostly independent of the other components and dominant in the winter months with heights exceeding 3 m, while being sporadic in the summer. The hindcast and the buoy measurements show good agreement in terms of the total energy for the mixed seas as well as the energy distribution among the components for in-depth investigation of weather and wave climate as well as its implications for wave resources.

4. Weather and wave patterns

The strong seasonal, multi-modal sea state around the Mariana Islands is a result of synoptic and mesoscale weather systems in different parts of the Western and Central Pacific. The National Weather Service reports the atmospheric and marine conditions daily in the Area Forecast Discussion (AFD) for Guam and the CNMI (https://mesonet.agron.iastate.edu/wx/afos/list.phtml). The historical AFD archive and the hindcast provide a basis for identifying typical weather and wave patterns in the region for understanding the sea state in terms of its components delineated by period. Figure 9 shows representative summer events with the CFSR surface wind and pressure as well as the hindcast significant wave height, peak period, and peak direction to demonstrate the met-ocean conditions. Among the synoptic weather phenomena in the region, trade winds are prevalent throughout the year (Eldredge, 1983, Jordan, 1955). They originate from a subtropical high ridge extending across the North Pacific with anti-cyclonic flows producing easterly winds toward the Mariana Islands. The trade winds are relatively gentle and uniform with periodic fluctuations during most of the summer. Figure 9a shows typical trade-wind conditions with steady moderate winds of 8 m/s in early July 2020. The seas around the islands, which are generated along an open fetch, are a result of the upstream flow and local winds at earlier and present time, respectively. The significant wave height of 1.5 m is quite uniform east of the islands, but decreases to 0.5 m off the sheltered west shores. Outside the sheltered waters, the peak period is consistent at 8 s, associated with the open fetch from the North Central Pacific to the Mariana Islands.

The summer trades near the Mariana Islands are sometimes interrupted by the monsoons originating from Southeast Asia (Becerro et al., 2006, Lander, 1996, Beattie and Elsberry, 2012, Lander and Guard, 2003). On July 30, 2018, the westerly monsoon flow with speeds of 7 m/s extends from the Philippines to the Mariana Islands (Fig. 9b). The event lasted for a few days with fully developed seas of 1.2 m significant wave height around Guam and the CNMI on August 1, 2018. The peak period increases from

7 to 9 s across the islands due to the increased fetch toward the east. Tropical cyclones occur typically in the summer and transition months (Holliday, 1975, Rupp and Lander, 1996) and influence the wave conditions around the Mariana Islands, even from a distance. As an example, Figure 9c shows the northwest migration of Typhoon Haisen away from the CNMI in early September 2020. It strengthens rapidly from September 3 to 4 and becomes a super-typhoon reaching category 4 strength with maximum 1-min sustained wind speeds above 69 m/s, but did not have a direct impact on the islands due to its location 1600 km away. The typhoon swells generated earlier traverse the open ocean to Mariana waters reaching 2.2 m wave height and 13 s peak period, except for the sheltered areas to the southeast where background seas of about 1 m and 9 s from the trade winds are dominant. Tropical cyclones which make direct landfall or pass near the islands can generate hazardous waves to the coastal communities.

In addition to trade-wind flows, mid-latitude cyclones and anticyclones migrating from west to east are rather common during the winter months (Harr et al., 2000). The resulting northerly swells and seas produce a notable contribution to the wave climate in the islands. Figure 10a shows a high-pressure system in the East China Sea on January 21, 2020, moving eastward to the north of the Mariana Islands 1.5 days later. The anticyclonic system produces northeasterly winds with speeds reaching 12 m/s across the islands that augment the easterly trades to generate heightened seas. Meanwhile, the low-pressure system east of the Kuril Islands strengthens and moves northeast toward the Kamchatka Peninsula. The low-pressure system with strong northwesterly winds generates swells reaching the Mariana islands. The combined significant wave height from seas and swells reaches 3.5 m on January 22, 2020. Around each island or island group, prominent shadows of the seas develop to the southwest with near-shore wave heights of less than 2.0 m. More extended shadows of the swell develop to the south of the islands at the same time. In contrast to the gradual transition of the significant wave height, the peak period shows a patchy distribution around the islands associated with shadowing of the multi-modal seas. The period of northeast seas from the nearby mid-latitude high increases from 8 s to 11 s along the fetch to the southwest. The background north swells with 14 s periods from the more distant mid-latitude low are visible off the western shores in the shadows of the moderate seas and to the east of the island chain.

The migrating mid-latitude systems can also generate northerly winds reaching the islands with influence on the local met-ocean conditions (Donets et al., 2018, Lander, 1994). In late January 2020, a low-pressure system east of Japan is accompanied by a high-pressure system at the East China Sea during the passage of an occluded cold front (Figure 10b). South-southeasterly winds prevail in the prefrontal atmosphere north of the Mariana Islands. As the high and low-pressure systems strengthen and move eastward, strong northwesterly winds sweep across the East China Sea bringing cold air from the mid-latitudes toward the tropics. The cold front reaches the Mariana islands with post-frontal northerly winds of 10 m/s on February 1. The post-frontal winds converge with moderate easterly trade winds of 6 m/s creating a shearline southeast of the islands. These near and far-field weather systems have profound influence on the complex local wave conditions. The significant wave height of the combined seas reaches 2.5 m west of the islands primarily due to the strong post-frontal northerly winds and decreases to 1.5 m on the east side, where the sea state can be mostly attributed to the moderate easterly seas augmented by north swells generated earlier by the low-pressure system east of the Kuril Islands. The distinct characteristics of each wave system can be identified in the peak period distribution. The short 5-7 s and long 14 s peak period west and east of the island chain, respectively, indicate wind waves from the frontal system and swells from the mid-latitude low-pressure system, while the intermediate 8-10 s period around the islands represents the combined effect of the easterly trade winds and northerly postfrontal winds. These typical weather systems and the corresponding wave fields provide a basis to elucidate the seasonal and spatial variations of the wave energy resources around the Mariana Islands.

The characteristics of the dominant wave components are best assessed using the partitioned hindcast. The IEC wave resources parameters, which are integrated from the entire spectrum, can be extended through spectral partitioning to provide a more complete description for multi-modal seas. The spectral partitions of the hindcast have already been validated with measurements from buoy 196. Figure 11 shows the six IEC parameters computed from the validated spectrum as well as its partitions for the three dominant wave components in 2017. The wave power and significant wave height time series have similar trends, but the former more clearly depicts the dominance of seas between 7 and 11 s due to the year-round occurrence of trade winds as well as their intensification by migrating mid-latitude high in the northwestern Pacific during the winter. The energy is occasionally augmented by swells with periods greater than 11 s from mid-latitude lows further north. The wind waves can have significant wave heights in the 0.5~2 m range, but only minor contributions to the total energy because of their short periods. The integrated energy period is close to the period for seas due to their primary contribution.

The spectral width parameter clearly differentiates the narrowband characteristics of the swells and the broadband wind waves. The seas have very consistent spectral width slightly above the swells. The same parameter for the combined sea state is noticeably larger than those of the individual components but is closer to the wind waves despite their low energy level throughout the year. This is complemented by the direction of the maximum directionally resolved wave power and the directionality coefficient, which correspond well to the characteristics of each component from a specific directional window. In the winter, eastward migration of mid-latitude lows and highs produces periodic direction changes for swells from north to northeast and seas from northeast to east. Wind waves throughout the year and seas in the summer are mainly from the east due to persistent trades albeit with occasional disruptions from tropical cyclones and monsoons. The results show wider directional spread of wind waves and seas due to their multiple sources, but more focused swells primarily from more distant low-pressure systems in the winter. Computation of the IEC parameters by spectral partition provides more pertinent information that can assist designers and operators to tune their devices for optimizing energy production in the strongly multimodal sea state around the Mariana Islands.

5. Seasonal wave resources

The validated long-term hindcast provides a wealth of information for analysis of the mixed seas and the individual components to understand the wave climate and resources. Figure 12 shows the average significant wave height and wave power as well as their intraannual variability. Averaged over the 42-year hindcast, the significant wave height is quite uniform across the region with a slight variation from 2.0 m to 1.8 m along the island chain from north to south. The wave height decreases to under 1 m off the western shores due to sheltering of the prevailing seas from easterly trade winds. This is important for the development of wave energy resources in the Mariana Islands because the western shores host major harbors and infrastructure, which can provide logistic support and serve as transportation hubs for deployment and maintenance. The wave conditions have large seasonal variations. Calmer trade winds occur in the boreal summer months of June, July, and August with about 1.5 m average significant wave height in the open ocean. Waves from tropical cyclones and summer monsoons can interrupt the moderate sea state and have minor contributions to the seasonal average due to their relatively low occurrence, but are enough to introduce faint shadows off the east shores. The trade winds and the resulting seas are strengthened by mid-latitude high-pressure systems in the northwestern Pacific during the boreal winter months of December to February. Frontal systems and mid-latitude low-pressure systems to the north also become active and produce severe wind waves and large swells impacting the Mariana Islands. Multi-modal seas become more frequent in winter with occasional treacherous conditions increasing the average significant wave height to above 2.4 m off the island shores. Such conditions are less favorable for installation and maintenance of wave energy devices and mooring systems.

The wave power is proportional to the square of wave height producing a larger contrast in the spatial distribution. The year-round average reaches 18 and 15 kW/m in the north and south with 10 kW/m in the shadows west of the islands. The Mariana Islands have steep insular slopes in the absence of shelves. The wave power in the deep water around islands increases linearly with the wave period to augment the seasonal variation. With mostly seas from westerly monsoons and east trade winds in the summer, the seasonal average is about 10 kW/m away from the islands and below 6 kW/m in the shadows off the west and east shores. In the winter months, the wave power reaches 26 and 22 kW/m in the northern and southern Mariana Islands primarily due to stronger easterly trade wind seas. The slight northward increase is a result of intermittent occurrences of north swells from mid-latitude low-pressure systems off the Kamchatka peninsula as well as northerly seas and wind waves from mid-latitude high-pressure systems and northwest frontal systems originating in the East China Sea. The north-facing shore experiences the most diverse wave climate as well as the highest energy level of each island. The wave power at the east and west shores is under 10 kW/m due to island sheltering. The overall increase of the significant wave height and wave power from the summer to winter in Guam and the CNMI is directly related to transition of the dominant weather systems in the Western and Central Pacific. Bulk parameters derived from the combined seas in Mariana waters do not always provide pertinent information for practical applications.

Performance of most wave energy conversion devices also depends on the wave period. The wave power can characterize the available wave resources but might not be sufficient for engineering design and operation planning. The mixed seas around the islands are generated by a range of synoptic and mesoscale processes in the Western and Central Pacific. The hindcast partitions allow separate analysis of each wave component defined by its period range. There are up to 10 partitions from the watershed algorithm for each hindcast spectrum in the SWAN output. We consider the three primary partitions by energy level and classify the computed wave height under the wind wave, seas, and swell categories based on the period being under 7 s, between 7 and 11 s, and above 11 s. When more than one partition is assigned to the same component at a time step, only the largest one is recorded to minimize noise from small and intermittent events and concatenated into a continuous sub-dataset. The three sub-datasets provide a basis for spatial and temporal analysis by dominant wave components. Figure 13 provides the average partitioned wave height for the occurrences in each category during the boreal summer and winter months. In contrast to the combined seas, the three components have distinct energy levels, patterns, and seasonality associated with climatology in the western and central Pacific.

The short-period wind waves are primarily generated by local winds with a relatively uniform distribution across the island chain. The summer has an average partitioned wave height of less than 0.6 m associated with the light to moderate easterly trades and southwesterly monsoon winds in the region. The partitioned wave height increases to 1.0 m from the strengthened trades and northerly frontal winds in the winter. In contrast, the intermediate-period seas are influenced by upstream trade wind flows with a longer fetch extending to the central Pacific. The average partitioned wave height reaches 1.1 m and 1.7 m on the windward side in the summer and winter, with a prominent reduction on the leeside to the west due to sheltering by the island chain. The long-period swells have distinct seasonal patterns due to the source location. Tropical cyclones are most active in the western Pacific during the summer months producing an average wave height of 1.3 m west of the island chain. The wave height from a tropical cyclone varies with the intensity, track, and forward speed, and the peak value could be much larger than the average. Mid-latitude cyclones occur to the north of the islands during the winter months. The average partitioned wave height of the swell reaches 1.5 m with a prominent shadow to the south. Similar to tropical cyclones, the peak swells could be much larger than the average. The seasonal distribution of individual wave components provides an additional level of detail for the description of wave climate and energy resources that assist selection and design of wave energy conversion devices for deployment near the Mariana Islands.

6. Discussion and Conclusions

The multimodal wave conditions in the Mariana Islands are influenced by local and distant weather systems in the Western and Central Pacific. An assessment of the recorded significant wave height, peak period, and peak direction identifies distinct components of wind waves, seas, and swells of below 7 sec, 7-11 sec, and above 11 sec, respectively. The 42-year hindcast, which was generated from reanalysis winds following the IEC TC-114 Technical Specification for a Class 2 (Feasibility) study, provides an effective approach to quantifying their spatial and temporal distributions around the islands for in-depth analysis of the wave climate and energy resources. The wave parameters and spectral partitions are thoroughly validated with measurements around the islands. The comparison with the altimetry observations shows good reproduction of the overall wave height and spatial pattern. The slight increase of RMSEs toward the west and north is associated with transition to more dynamic weather systems from the Central to the Western Pacific. In comparison with buoy records, the wave hindcast shows slight overestimation for the small events and underestimation for the peaks of large events, while demonstrating good agreement for the energy distribution among the dominant wave components in the multi-modal sea state. Although the demarcation of wind waves, seas, and swells is not always well defined as with the atmospheric forcing and is location or event dependent, the good correlation obtained in the spectral partitions ensures that the selected period ranges can capture the dominant energy in the subsequent analysis.

The validated hindcast and partitioned parameters provide details in the temporal and spatial distributions of the wind waves, seas, and swells. The year-round trade winds, driven by a subtropical ridge, account for the prevailing and background seas that play a significant role in the local wave climatology. The sea state is gentler with the prevailing direction from the east in the summer and can be augmented on the leeside of the islands by seas from monsoons as well as swells from tropical cyclones to the west even at some distance away. In the winter months, the trade wind waves are energized by northeasterly winds from mid-latitude high-pressure systems and augmented by swells from the mid-latitude low-pressure systems to the north. In addition, frontal systems can reach the Mariana Islands from the northwest generating short-period wind waves with large amplitude on the west side of the islands. These local and distant weather systems bring waves of various occurrence frequencies accounting for the seasonal variation of significant wave height, peak period, and energy level. The wave components from different directions are sheltered by the islands leading to complex spatial variations. Implementation of the IEC wave energy resource parameters by spectral partition is an effective approach to describe the multi-modal sea state with distinct energy characteristics for each component.

The 42-year wave hindcast provides valuable insights into the wave resources along the island chain in support of energy converter design and planning. The wave power has strong seasonal variation due to transition between near and far-field weather systems affecting both the wave height and period. The summer has an average around 10 kW/m associated with light to moderate trade winds, despite occasional large events from tropical cyclones and monsoons. The sea state becomes more treacherous in the winter months with average wave power up to 22 kW/m around the islands. Despite having different energy levels in the two seasons, the northern portion of the island archipelago has slightly greater energy resources. Around each Island, the energy level decrease dramatically off the west shores because of sheltering of persistent trade wind waves and seasonal north swells. The north-facing shores of Saipan, Rota, and Guam have the most diverse energy resources comparable to those in the open ocean due to direct exposure to seas all year round as well as strong wind waves and swells in the winter. The available wave power, which meets the requirements of most energy converters, is at a short distance from shores due to the steep insular slope and the absence of shelves. However, candidate energy converters should be adaptable over the wide range of peak periods and directions to be viable for the Mariana Islands.

The PNNL hindcast has been proven to be a valuable dataset for wave climate research and energy resource assessment through the present study with the Mariana Islands as well as the corresponding studies for American Samoa (García Medina et al., 2023) and Hawaii (Li et al., 2021). The Mariana Islands experience the most diverse wave conditions among the studied regions due to their location in a typhoon spawning area as well as the presence of monsoons and cold fronts from the western Pacific Rim. The dataset covers all US and affiliated Pacific islands, in which the ocean has a significant role in the livelihood of local communities. The archived model output of bulk and partitioned parameters within the EEZs and frequency-direction spectra near the shore is meant to support a wide variety of scientific and engineering applications. The 100-m resolution on an unstructured grid provides a long-term description of the nearshore wave environment that influences coastal circulation, sediment transport, and mixing processes. The spectral data can provide boundary conditions for phrase-averaged or phase-resolving modeling of coastal waves and circulations at much higher resolution at the shore. The full hindcast dataset, which will be publicly available online, can be implemented in studies related to coastal hazards, shoreline erosion, maritime operations, and coral reef ecosystems.

Acknowledgement

This research is supported by the US Department of Energy, Office of Energy Efficiency and Renewable Energy, Water Power Technologies Office under contract DE-AC05-76RL01830 to Pacific Northwest National Laboratory (PNNL). Model simulations were performed using PNNL's and National Renewable Energy Laboratory Institutional Computing facilities. The authors thank the external steering committee, chaired by Dr. Bryson Robertson, for providing technical oversight to the development of the wave hindcast that covers the US and affiliated Pacific islands and the two anonymous reviewers for the comments and suggestions on the manuscript.

References:

A. Chawla, S. Deanna, T. Hendrik, 30 Year Wave Hindcasts using WAVEWATCH III with CFSR winds, Phase 1. NOAA/NWS/NCEP/MMAB. Maryl. USA 23, 2012.

A. Ribal, I.R. Young, 33 years of globally calibrated wave height and wind speed data based on altimeter observations. *Sci Data 6*, 77 (2019). https://doi.org/10.1038/s41597-019-0083-9.

S. Ahn, V.S. Neary, K. A. Haas, Global wave energy resource classification system for regional energy planning and project development. *Renewable and Sustainable Energy Reviews,* 162 (2022), 112438. https://doi.org/10.1016/j.rser.2022.112438.

C. Bosserelle, S. Reddy, D. Lal, WACOP wave climate reports. Guam, Guam. Secretariat of the Pacific Community. 2015, http://gsd.spc.int/wacop/.

C.R. Holliday, Tropical Cyclones Affecting Guam. FLEET WEATHER CENTRAL/JOINT TYPHOON WARNING CENTER FPO SAN FRANCISCO 96630, 1975.

C.L. Jordan, Some features of the rainfall at Guam. *Bulletin of the American Meteorological Society*, 36(1955), 446-455, https://doi.org/10.1175/1520-0477-36.9.446.

D. P. Dee, S. M. Uppala, A. J. Simmons, P. Berrisford, P. Poli, S. Kobayashi, U. Andrae, M. A. Balmaseda, G. Balsamo, P. Bauer, P. Bechtold, A. C. M. Beljaars, L. van de Berg, J. Bidlot, N. Bormann, C. Delsol, R. Dragani, M. Fuentes, A. J. Geer, L. Haimberger, S. B. Healy, H. Hersbach, E. V. Hólm, L. Isaksen, P. Kållberg, M. Köhler, M. Matricardi, A. P. McNally, B. M. Monge-Sanz, J.-J. Morcrette, B.-K. Park, C. Peubey, P. de Rosnay, C. Tavolato, J.-N. Thépaut, F. Vitart , The ERA-Interim reanalysis: Configuration and performance of the data assimilation system, *Quarterly Journal of the royal meteorological society*, 137 (2011), 553-597, https://doi.org/10.1002/qj.828.

C. Dutheil, S. Jullien, J. Aucan, C. Menkes, R. Le Gendre, and S. Andréfouët, The wave regimes of the Central Pacific Ocean with a focus on pearl farming atolls, *Marine Pollution Bulletin* 162 (2021): 111751. https://doi.org/10.1016/j.marpolbul.2020.111751.

F. Ardhuin, E. Rogers, A.V. Babanin, J.-F. Filipot, R. Magne, A. Roland, A. van der Westhuysen, P. Queffeulou, J.-M. Lefevre, L. Aouf, F. Collard, Semiempirical Dissipation Source Functions for Ocean Waves. Part I: Definition, Calibration, and Validation. *Journal of Physical Oceanography,* 40 (2010), 1917–41. https://doi.org/10.1175/2010JPO4324.1.

G. G. Medina, Z. Yang, Z., N. Li, K.F. Cheung, H. Wang, F.M. Ticona Rollano, High-Resolution Regional Wave Hindcast for US Pacific Island Territories (No. PNNL-31208). Pacific Northwest National Lab (PNNL), Richland, WA (United States), 2021.

G. G. Medina, Z. Yang, W.-C. Wu, T. Wang, Wave resource characterization at regional and nearshore scales for the U.S. Alaska coast based on a 32-year high-resolution hindcast. Renewable Energy, 170 (2021), 595–612. https://doi.org/10.1016/j.renene.2021.02.005.

G. G. Medina, Z. Yang, N. Li, K.F. Cheung, T. Wang, and W. Wu., High-Resolution Regional Wave Hindcast for Hawaii. PNNL-29370. Richland, WA: Pacific Northwest National Laboratory. High-Resolution Regional Wave Hindcast for Hawaii, 2019.

G. G. Medina, Z. Yang, N. Li, K.F. Cheung, E. Luto-McMoore, Wave climate and energy resources in American Samoa from a 42-year hindcast. *Renewable Energy*, in review.

G.J. Komen, L. Cavaleri, M. Donelan, K. Hasselmann, S. Hasselmann and P. A. E. M. Janssen, Dynamics and Modelling of Ocean Waves. Cambridge University Press, 1994.

J. L. Hanson, O. M. Phillips, Automated analysis of ocean surface directional wave spectra, *Journal of Atmospheric and Oceanic Technology,* 18 (2001), 277–93. https://doi.org/10.1175/1520-0426(2001)018<0277:AAOOSD>2.0.CO;2.

H. Hersbach, B. Bell, P. Berrisford, S. Hirahara, A. Horányi, J. Muñoz-Sabater, J. Nicolas, C. Peubey, R. Radu, D. Schepers, A. Simmons, C. Soci, S. Abdalla, X. Abellan, G. Balsamo, P. Bechtold, G. Biavati, J. Bidlot, M. Bonavita, G. D. Chiara, P. Dahlgren, D. Dee, M. Diamantakis, R. Dragani, J. Flemming, R. Forbes, M. Fuentes, A. Geer, L. Haimberger, S. Healy, R. J. Hogan, E. Hólm, M. Janisková, S. Keeley, P. Laloyaux, P. Lopez, C. Lupu, G. Radnoti, P. de Rosnay, I. Rozum, F. Vamborg, S. Villaume, J.-N. Thépaut The ERA5 global reanalysis. *Quarterly Journal of the Royal Meteorological Society*, 146(2020), 1999-2049. https://doi.org/10.1002/qj.3803.

H.L. Tolman, D. Chalikov, Source terms in a third-generation wind-wave model, *J. Phys. Oceanogr*, 26 (1996), 2497-2518. https://doi.org/10.1175/1520-0485(1996)026%3C2497:STIATG%3E2.0.CO;2.

H.L. Tolman, Development of a multi-grid version of WAVEWATCH III. NOAA / NWS / NCEP / MMAB Technical Note 256, 2006.

H.L. Tolman, A mosaic approach to wind wave modeling, *Ocean Modelling*, 25 (2008), 35-47. https://doi.org/10.1016/j.ocemod.2008.06.005

H.L. Tolman, User manual and system documentation of WAVEWATCH III version 3.14. NOAA / NWS / NCEP / MMAB Technical Note 276, 2009.

J. Portilla-Yandún, C. Luigi, J.P. Van Vledder, Wave spectra partitioning and long term statistical distribution. *Ocean Modelling*, 96 (2015), 148-160. https://doi.org/10.1016/j.ocemod.2015.06.008

J. Portilla-Yandún, J. Edwin, Covariate extreme value analysis using wave spectral partitioning. Journal of Atmospheric and Oceanic Technology 37.5 (2020), 873-888. https://doi.org/10.1175/JTECH-D-19-0198.1

J.A. Rupp, M.A. Lander, A technique for estimating recurrence intervals of tropical cyclone-related high winds in the tropics: Results for Guam. Journal of Applied Meteorology and Climatology, 35(1996), 627-637. https://doi-org.eres.library.manoa.hawaii.edu/10.1175/1520-0450(1996)035%3C0627:ATFERI%3E2.0.CO;2

J.C. Beattie, R.L. Elsberry, Western North Pacific monsoon depression formation. Weather and forecasting, 27(2012), 1413-1432. https://doi-org.eres.library.manoa.hawaii.edu/10.1175/WAF-D-11-00094.1

J.E. Stopa, K.F. Cheung, Periodicity and pattern of ocean wind and wave climate. *Journal of Geophysical Research: Oceans*, 119(2014), 5563–5584. https://doi.org/10.1002/2013JC009729.

J.E. Stopa, K.F. Cheung, Intercomparison of wind and wave data from the ECMWF Reanalysis Interim and NCEP Climate Forecast System Reanalysis. *Ocean Modelling*, 75 (2014), 65-83. https://doi.org/10.1016/j.ocemod.2013.12.006.

J.E. Stopa, J.E., K.F. Cheung, Y.L. Chen, Assessment of wave energy resources in Hawaii. *Renewable Energy,* 36(2011), 554-567. https://doi.org/10.1016/j.renene.2010.07.014.

L.G. Eldredge, Summary of environmental and fishing information on Guam and the Commonwealth of the Northern Mariana Islands: historical background, description of the islands, and review of the climate, oceanography, and submarine topography. 1983

M.A. Becerro, V. Bonito, V.J. Paul, Effects of monsoon-driven wave action on coral reefs of Guam and implications for coral recruitment. *Coral Reefs*, 25 (2006), 193-199.

M. Zijlema, Computation of wind-wave spectra in coastal waters with SWAN on unstructured grids. *Coastal Engineering*, *57*(2010), 267-277. https://doi.org/10.1016/j.coastaleng.2009.10.011.

M.A., Lander, Meteorological factors associated with drought on Guam (No. 75). Water and Energy Research Institute of the Western Pacific, 1994.

M.A. Lander, C.P. Guard, Creation of a 50-year rainfall database, annual rainfall climatology, and annual rainfall distribution map for Guam. Mangilao, GU, USA: Water and Environmental Research Institute of the Western Pacific, University of Guam, 2003.

M.A. Lander, Specific tropical cyclone track types and unusual tropical cyclone motions associated with a reverse-oriented monsoon trough in the western North Pacific. Weather and Forecasting, 11(1996), 170-186. https://doi-org.eres.library.manoa.hawaii.edu/10.1175/1520-0434(1996)011%3C0170:STCTTA%3E2.0.CO;2

M.N. Allahdadi, B. Gunawan, J. Lai, R. He, V.S. Neary, Development and validation of a regional-scale high-resolution unstructured model for wave energy resource characterization along the US East Coast. *Renewable Energy*, *136 (2019)*, 500-511. https://doi.org/10.1016/j.renene.2019.01.020.

N. Li, K.F. Cheung, J.E. Stopa, F. Hsiao, Y.-L. Chen, L. Vega, P. Cross, Thirty-four years of Hawaii wave hindcast from downscaling of climate forecast system reanalysis, *Ocean Modelling,* 100 (2016), 78-95. https://doi.org/10.1016/j.ocemod.2016.02.001.

N. Li, G. García-Medina, K.F. Cheung, Z. Yang, Wave energy resources assessment for the multi-modal sea state of Hawaii. *Renewable Energy*, *174(2021)*, 1036-1055. https://doi.org/10.1016/j.renene.2021.03.116.

N. Booij, L.H. Holthuijsen, R.C. Ris, The" SWAN" wave model for shallow water. *Coastal Engineering 1996*, 668-676. https://doi.org/10.1061/9780784402429.053.

N.R.R.C. Booij, R.C. Ris, L.H. Holthuijsen, A third-generation wave model for coastal regions: 1. Model description and validation, *Journal of geophysical research: Oceans*, *104*(1999), 7649-7666. https://doi.org/10.1029/98JC02622.

P.A. Harr, R.L. Elsberry, T.F. Hogan, Extratropical transition of tropical cyclones over the western North Pacific. Part II: The impact of midlatitude circulation characteristics. Monthly weather review, 128(2000), 2634-2653. https://doi-org.eres.library.manoa.hawaii.edu/10.1175/1520-0493(2000)128%3C2634:ETOTCO%3E2.0.CO;2

S. Ahn, A.H. Kevin, V. S. Neary. Wave Energy Resource Characterization and Assessment for Coastal Waters of the United States. *Applied Energy,* 267 (2020): 114922. https://doi.org/10.1016/j.apenergy.2020.114922.

S. Saha, S. Moorthi, H. Pan, X. Wu, J. Wang, S. Nadiga, P. Tripp, R. Kistler, J. Woollen, D. Behringer, H. Liu, D. Stokes, R. Grumbine, G. Gayno, J. Wang, Y.-T. Hou, H.-Y. Chuang, H.-M. H. Juang, J. Sela, M. Iredell, R. Treadon, D. Kleist, P. V. Delst, D. Keyser, J. Derber, M. Ek, J. Meng, H. Wei, R. Yang, S. Lord, H. van den Dool, A. Kumar, W. Wang, C. Long, M. Chelliah, Y. Xue, B. Huang, J.-K. Schemm, W. Ebisuzaki, R. Lin, P. Xie, M. Chen, S. Zhou, W. Higgins, C.-Z. Zou, Q. Liu, Y. Chen, Y. Han, L. Cucurull, R. W. Reynolds, G. Rutledge, M. Goldberg, The NCEP Climate Forecast System Reanalysis. *Bulletin of the American Meteorological Society,* 91 (2010), 1015–58. https://doi.org/10.1175/2010BAMS3001.1.

S. Saha, S. Moorthi, X. Wu, J. Wang, S. Nadiga, P. Tripp, D. Behringer, Y.T. Hou, H.Y. Chuang, M. Iredell, M. Ek, The NCEP climate forecast system version 2. *Journal of climate*, *27*(2014), 2185-2208. https://doi.org/10.1175/JCLI-D-12-00823.1.

T. Durrant, D. Greenslade, M. Hemer, C. Trenham, A global wave hindcast focussed on the Central and South Pacific*, Centre for Australian Weather and Climate Research Tech. Rep.*, 54 (2014), 1917-1941.

T. Durrant, M. Hemer, G. Smith, C. Trenham, D. Greenslade, CAWCR Wave Hindcast - Aggregated Collection. v5. CSIRO. Service Collection, 2019. http://hdl.handle.net/102.100.100/137152?index=1.

T. Durrant, D. Greenslade, M. Hemer, C. Trenham, A global wave hindcast focussed on the Central and South Pacific, 40(2014), 1917-1941.

U. Ulbrich, G.C. Leckebusch, J.G. Pinto, Extra-tropical cyclones in the present and future climate: a review. *Theoretical and Applied Climatology*, 96(2009), 117–131. https://doi.org/10.1007/s00704-008-0083-8

V. Donets, E.L. Atlas, L.L. Pan, S.M. Schauffler, S. Honomichl, R.S. Hornbrook, E.C. Apel, T. Campos, S.R. Hall, K. Ullmann, J.F. Bresch, Wintertime transport of reactive trace gases from East Asia into the deep tropics. Journal of Geophysical Research: Atmospheres, 123(2018), pp.12-877. https://doi-org.eres.library.manoa.hawaii.edu/10.1029/2017JD028231

W. Wu, T. Wang, Z. Yang, and G. García-Medina, Development and Validation of a High-Resolution Regional Wave Hindcast Model for U.S. West Coast Wave Resource Characterization, *Renewable Energy,* 152 (2020), 736–53. https://doi.org/10.1016/j.renene.2020.01.077.

WAMDIG, The WAM model - A third generation ocean wave prediction model, *Journal of Physical Oceanography*, 18 (2009), 1775-1810. https://doi.org/10.1175/1520-0485(1988)018%3C1775:TWMTGO%3E2.0.CO;2.

J. Yang, and J. Zhang. Validation of Sentinel-3A/3B satellite altimetry wave heights with buoy and Jason-3 data. *Sensors*, 19 (2019), 2914. https://doi.org/10.3390/s19132914.

Y.Y. Chao, L. D. Burroughs, H. L. Tolman, Wave forecasting for the Eastern North Pacific and adjacent waters. NWS/NCEP Technical Procedures Bulletin 491 (2003).

Y.Y. Chao, L. D. Burroughs, H. L. Tolman, Wave forecasting for the Western North Atlantic and adjacent waters. NWS/NCEP Technical Procedures Bulletin 495 (2003).

Z. Yang, G. García-Medina, W. Wu, T. Wang. Characteristics and Variability of the Nearshore Wave Resource on the U.S. West Coast, *Energy*, 203 (2020), 117818. https://doi.org/10.1016/j.energy.2020.117818.

Z. Yang, V. S. Neary, T. Wang, B. Gunawan, A. R. Dallman, and W. Wu., A Wave Model Test Bed Study for Wave Energy Resource Characterization, *Renewable Energy*, Wave *and Tidal Resource Characterization*, 114 (2017), 132–44. https://doi.org/10.1016/j.renene.2016.12.057.

Z. Yang, W. Wu, T. Wang, and L. Castrucci. High-Resolution Regional Wave Hindcast for the U.S. West Coast, 2018. https://doi.org/10.2172/1573061.

Z. Yang, W. Wu, T. Wang, G. García Medina, and L. Castrucci, High-Resolution Regional Wave Hindcast for the U.S. Alaska Coast, 2019. https://doi.org/10.2172/1579259.

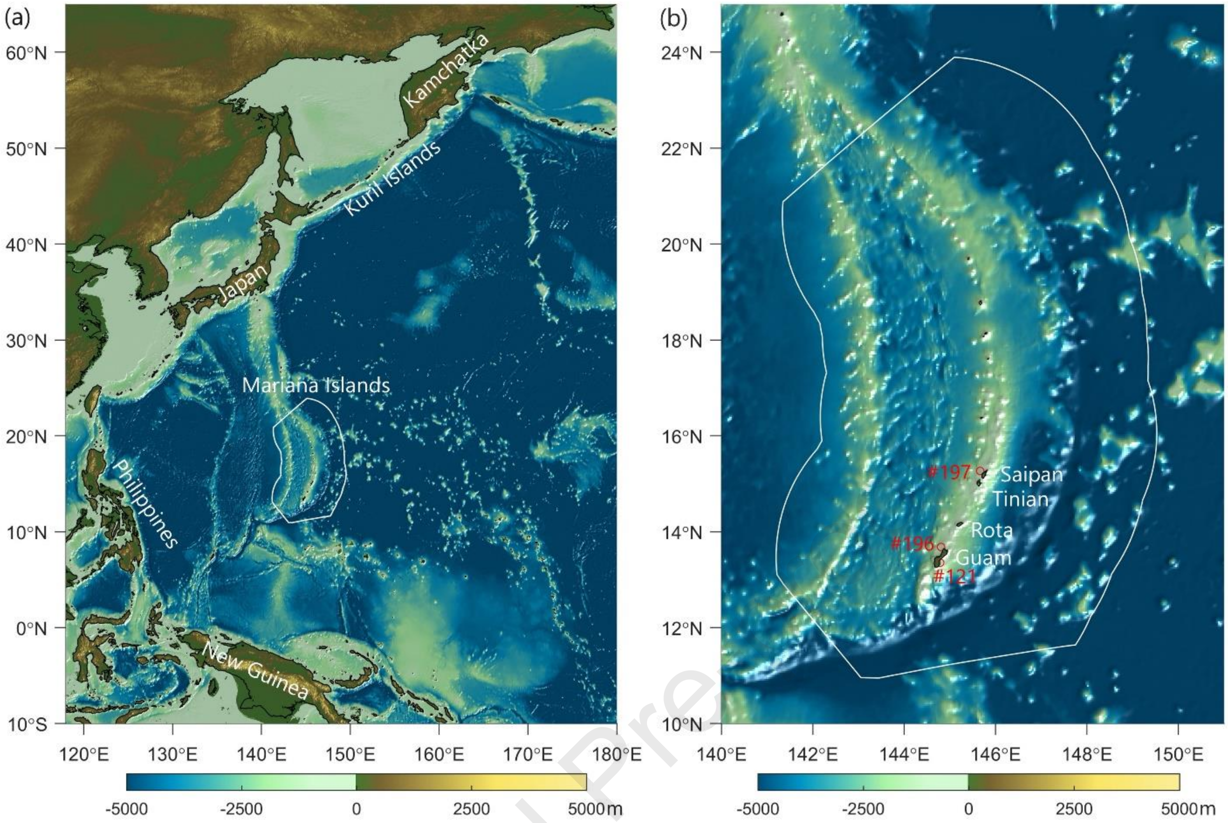

Figure 1. Location and bathymetric maps. (a) Western and central Pacific. (b) Mariana Islands. The red circles and labels indicate CDIP buoys. The white line delineates the Exclusive Economic Zone.

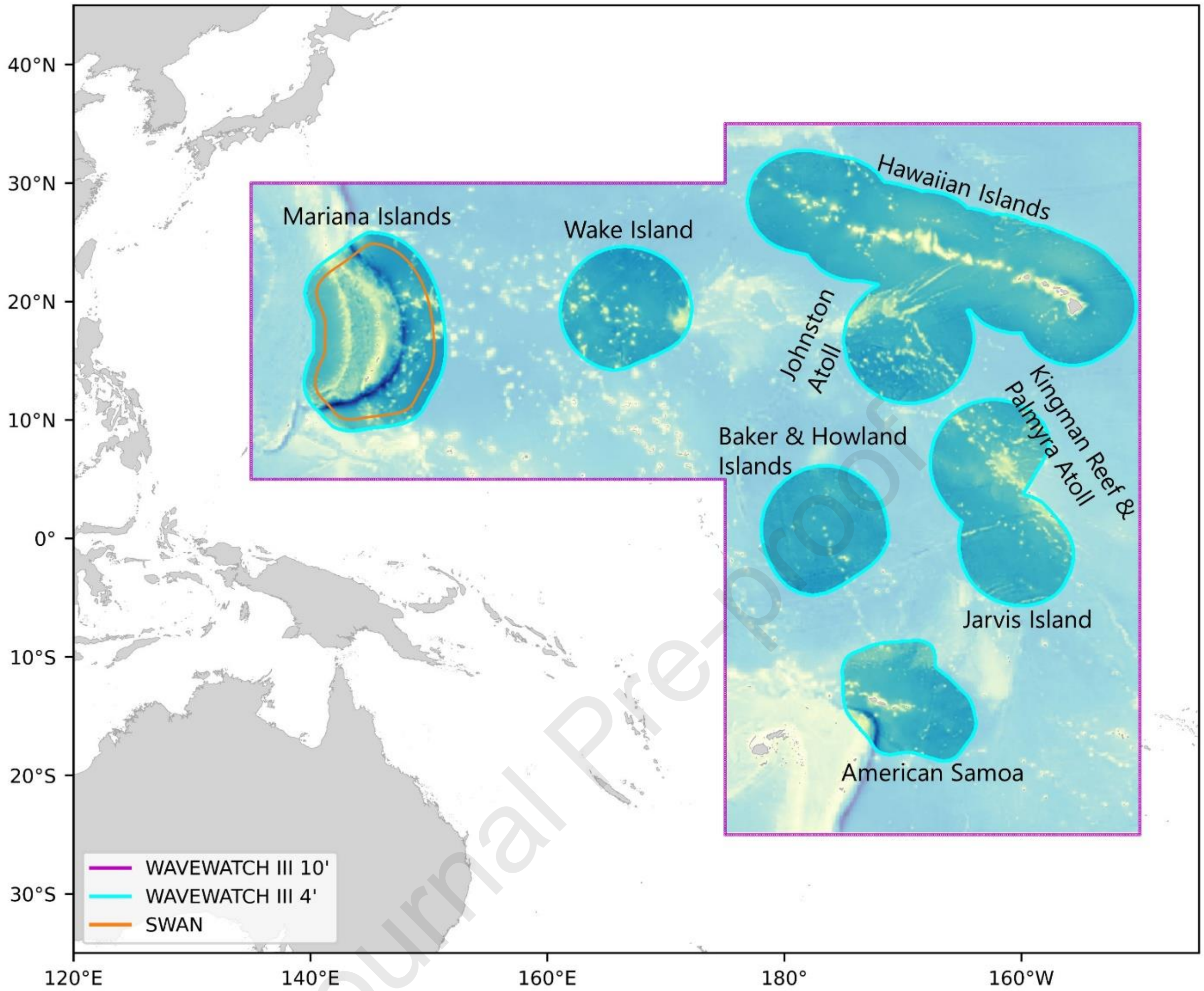

Figure 2. Regional WAVEWATCH III nested grids for the Pacific Islands and the SWAN unstructured grid for the Mariana Islands.

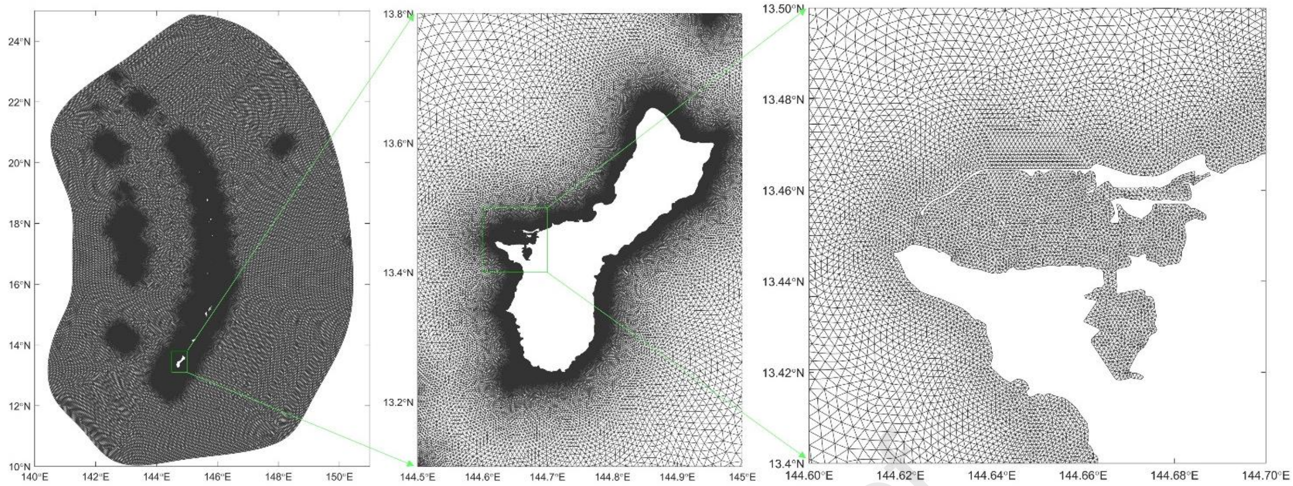

Figure 3. Telescopic views of the SWAN unstructured grid with resolution from 5 km at the boundary to 100 m at the shore.

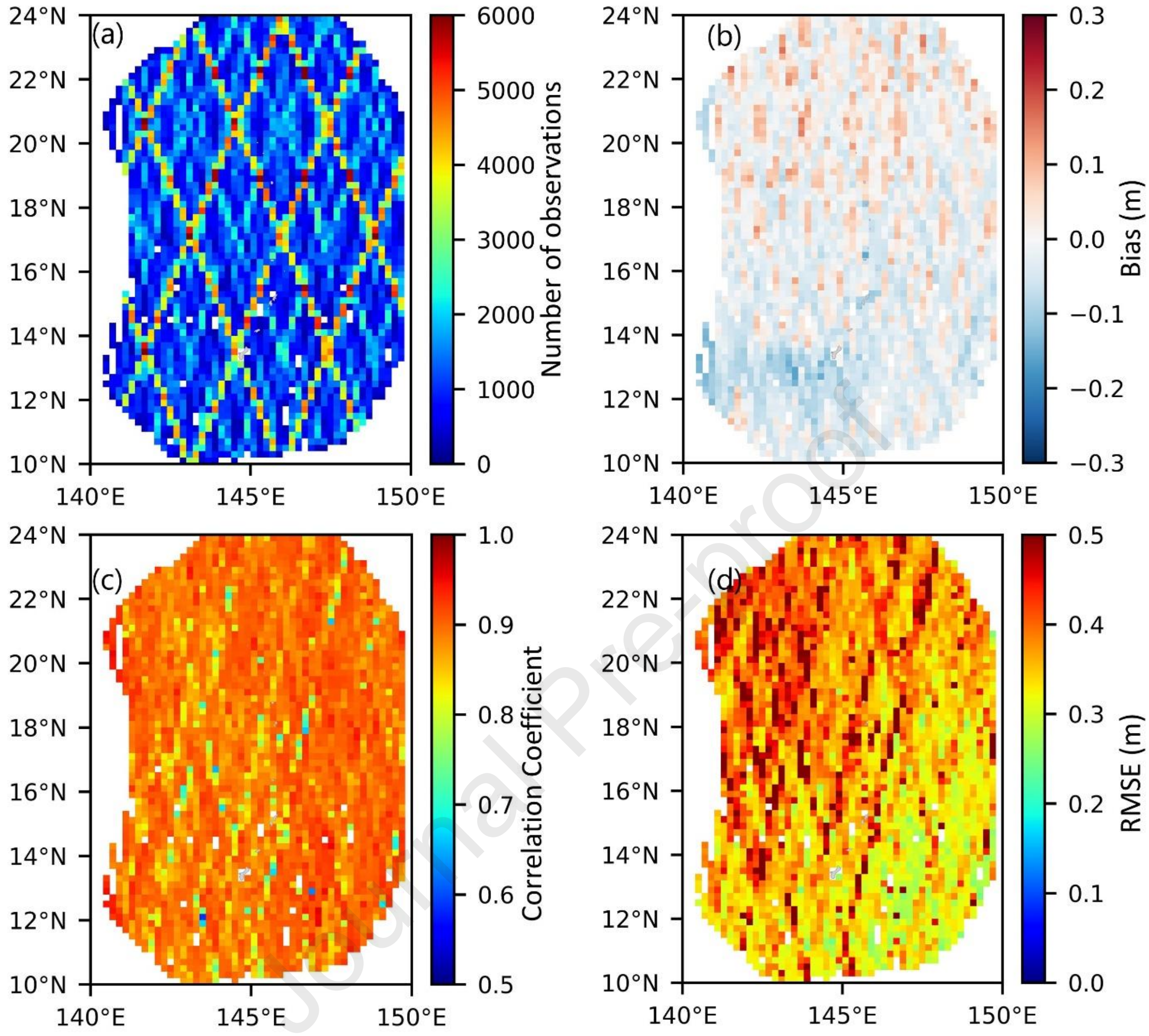

Figure 4. Comparison between hindcast and altimetry observations. (a) Bins and data density over the SWAN domain. (b) Bias. (c) Correlation Coefficient. (d) Root-mean-square error (RMSE).

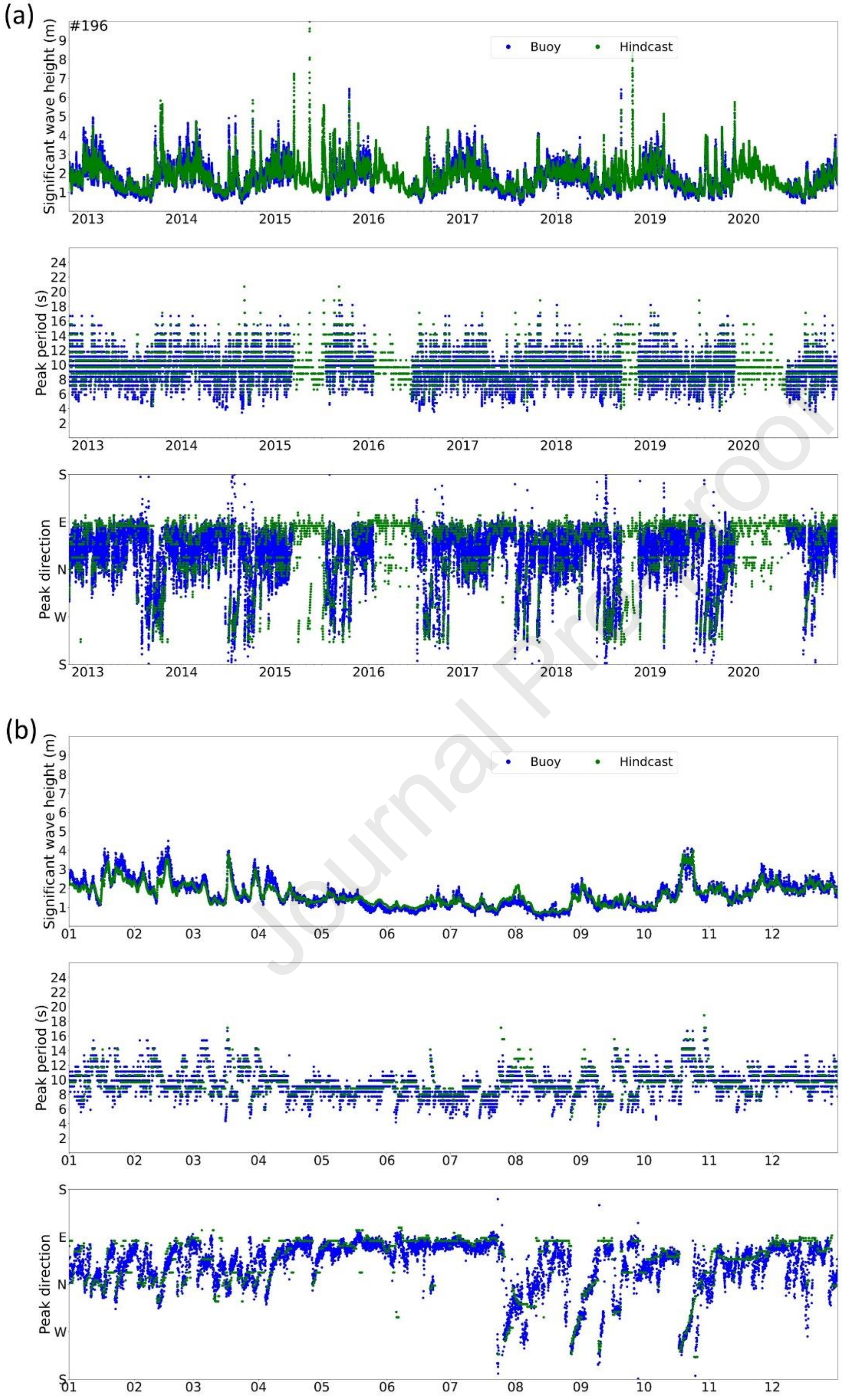

Figure 5. Time series of significant wave height, peak period, and direction from buoy #196 and the wave hindcast (a) from 2013 to 2020 and (b) in 2017.

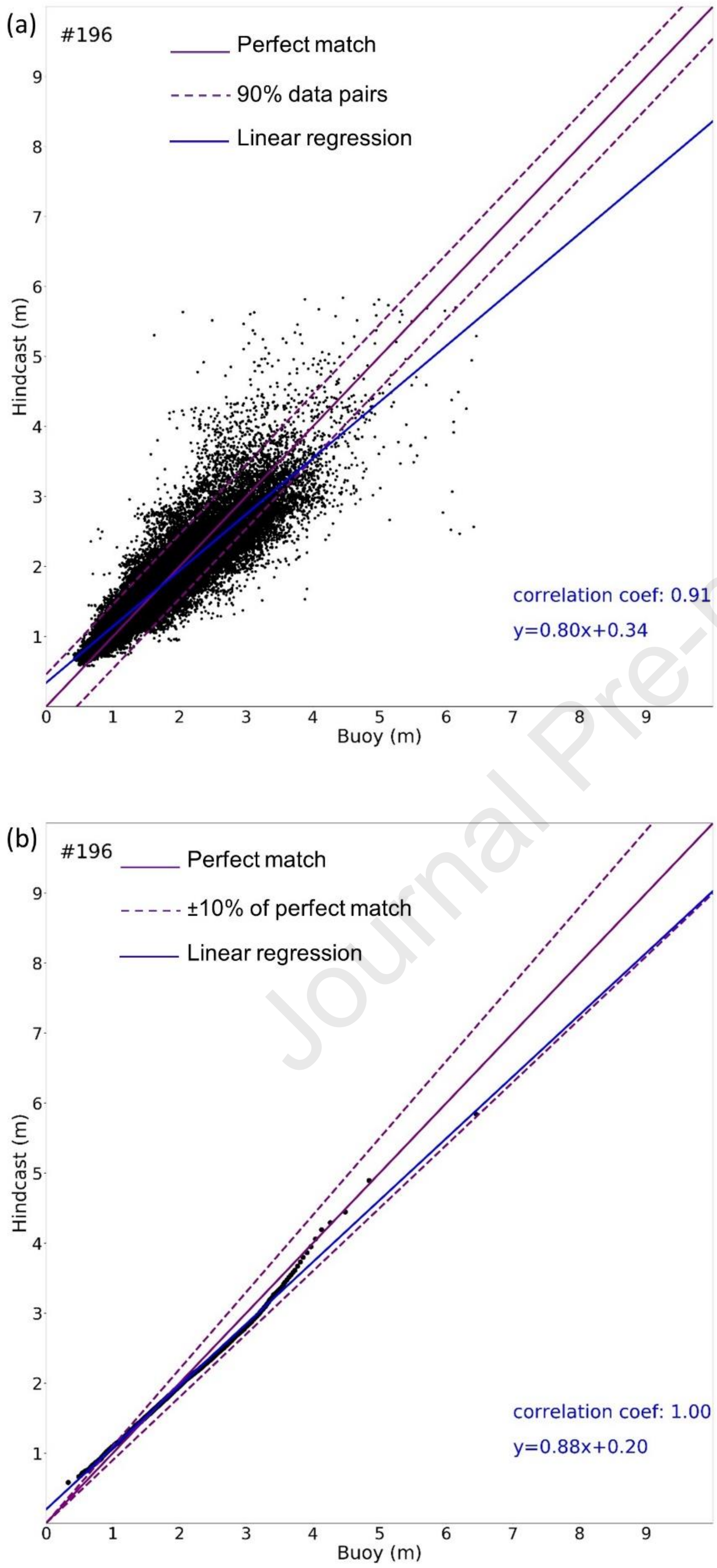

Figure 6. Scatter and Q-Q plots of measured and hindcast significant wave height at buoy #196.

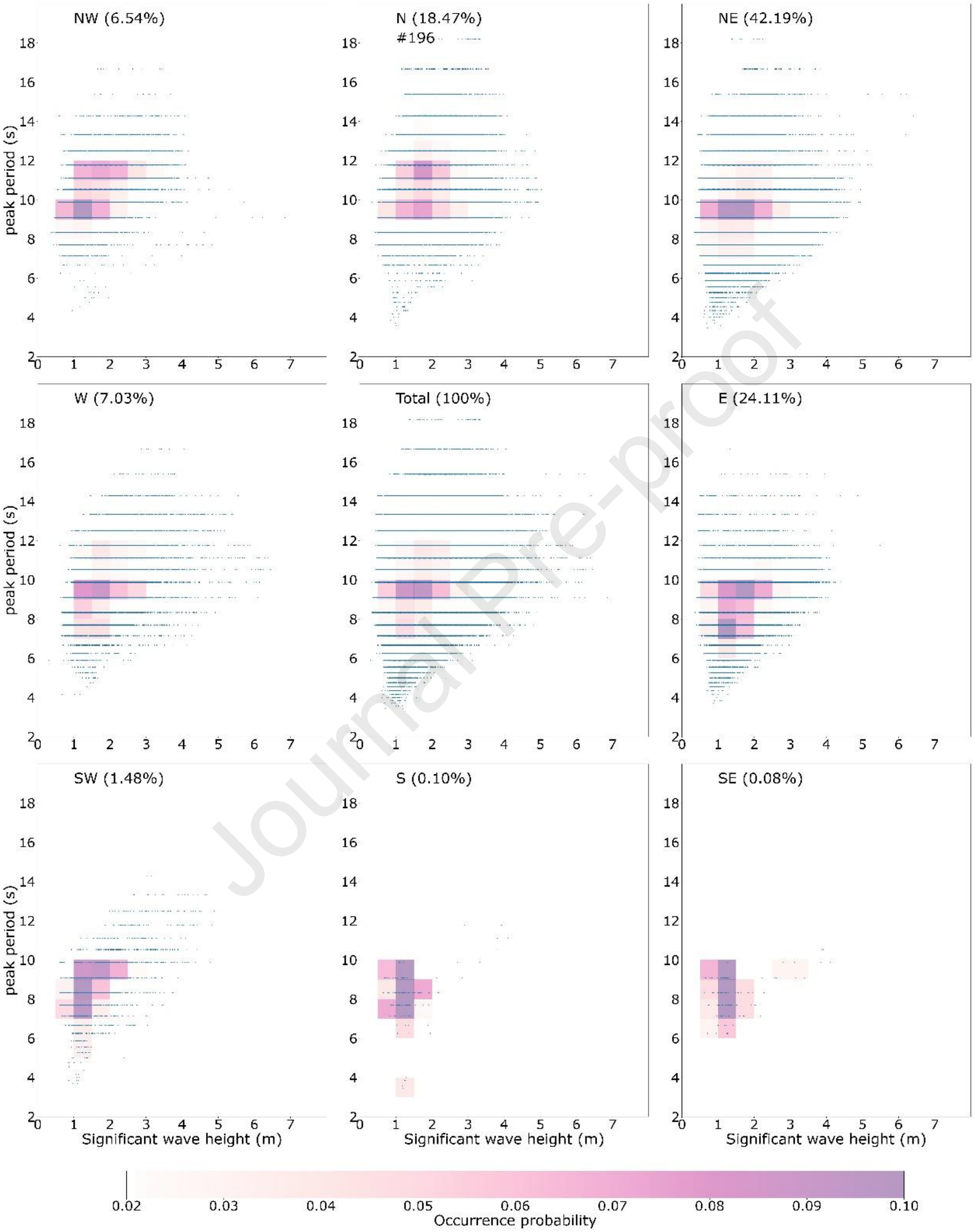

Figure 7. Scatter diagram for the measured significant wave height and peak period in eight directional windows from buoy #196.

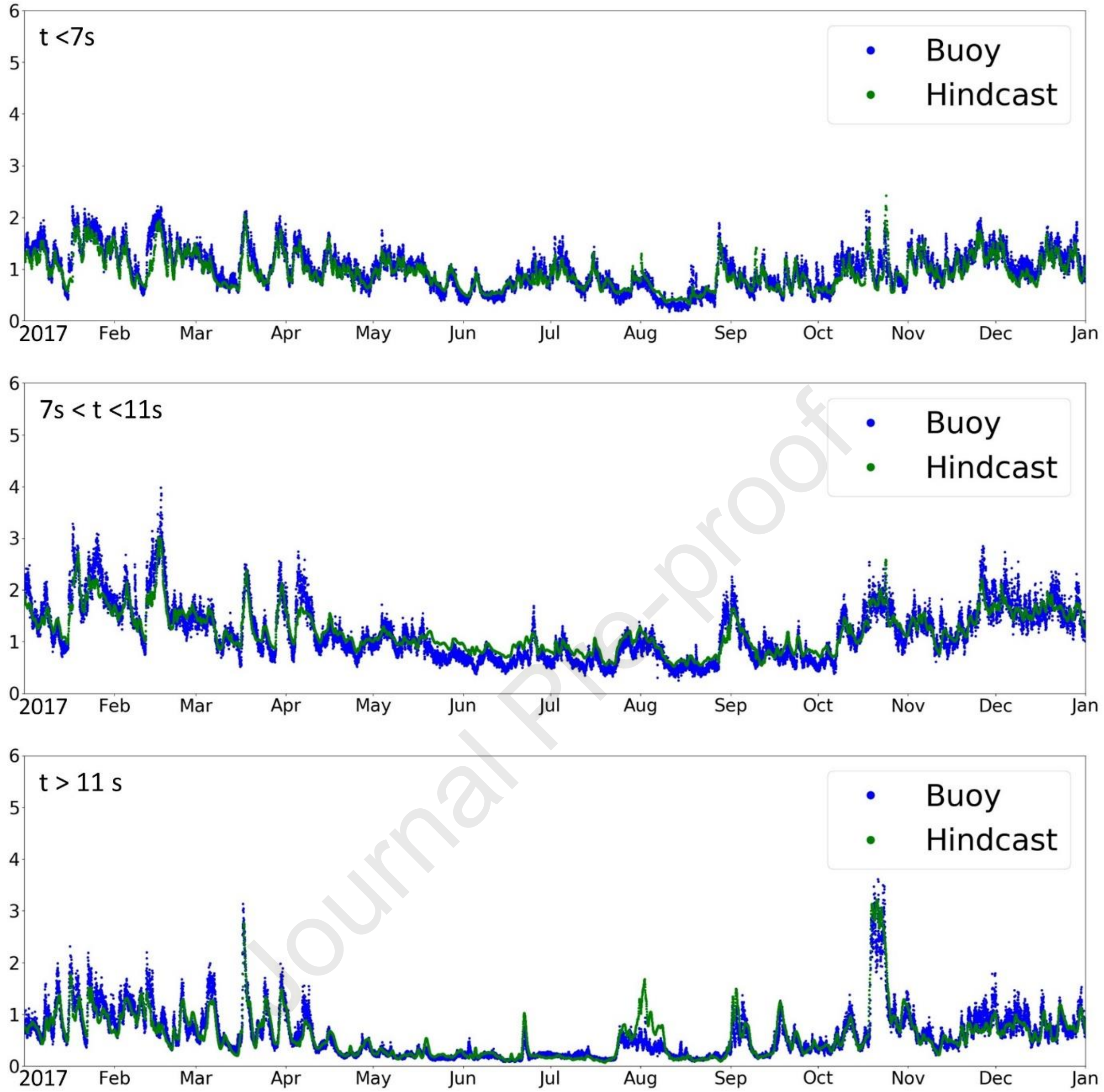

Figure 8. Time series of representative wave heights for periods less than 7s, 7-11 s, and above 11 s at buoy #196 in 2017.

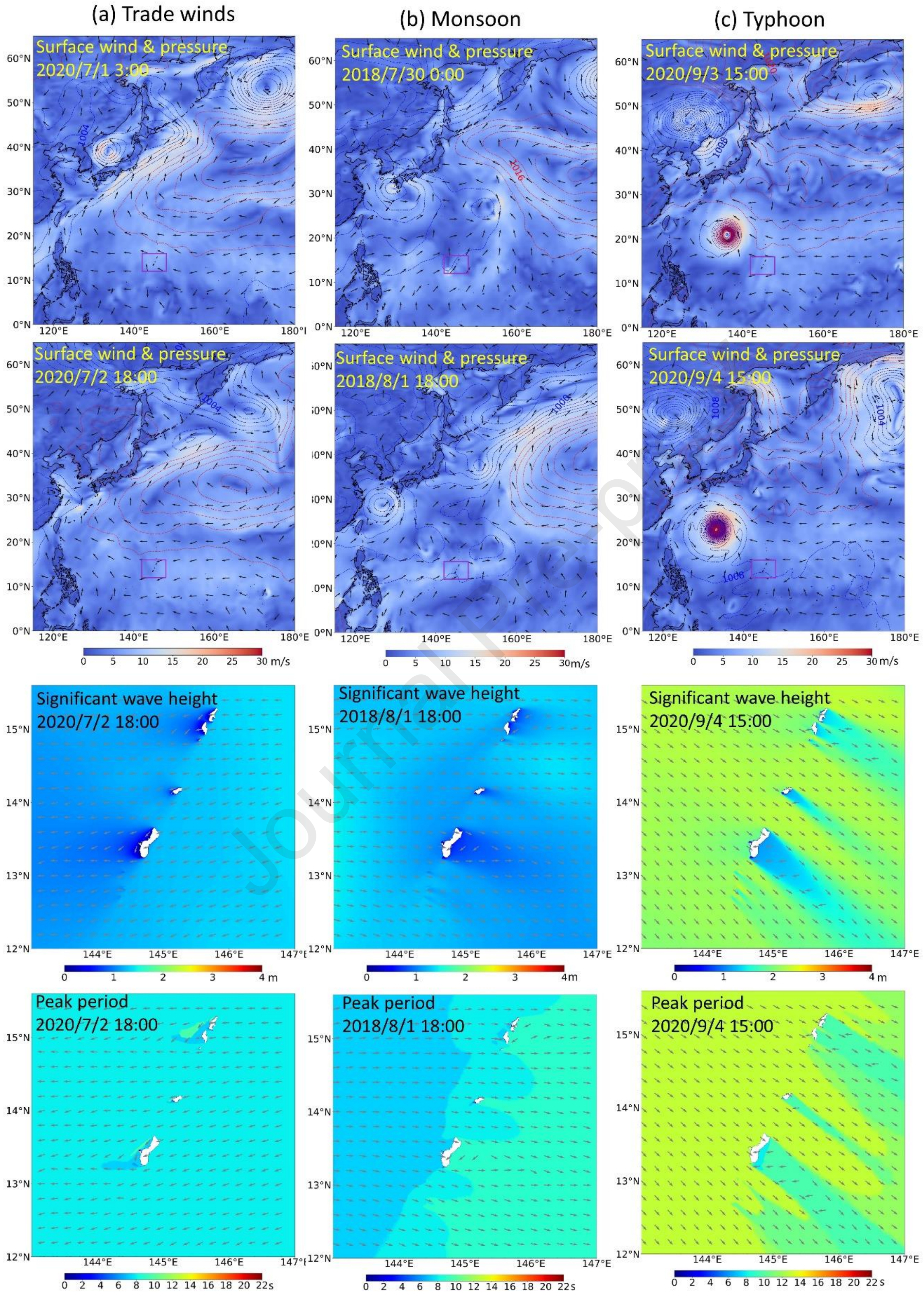

Figure 9. Representative summer weather systems in the Western and Central Pacific and wave patterns near Guam and the CNMI. (a) Trade winds. (b) Monsoon. (c) Tropical cyclone.

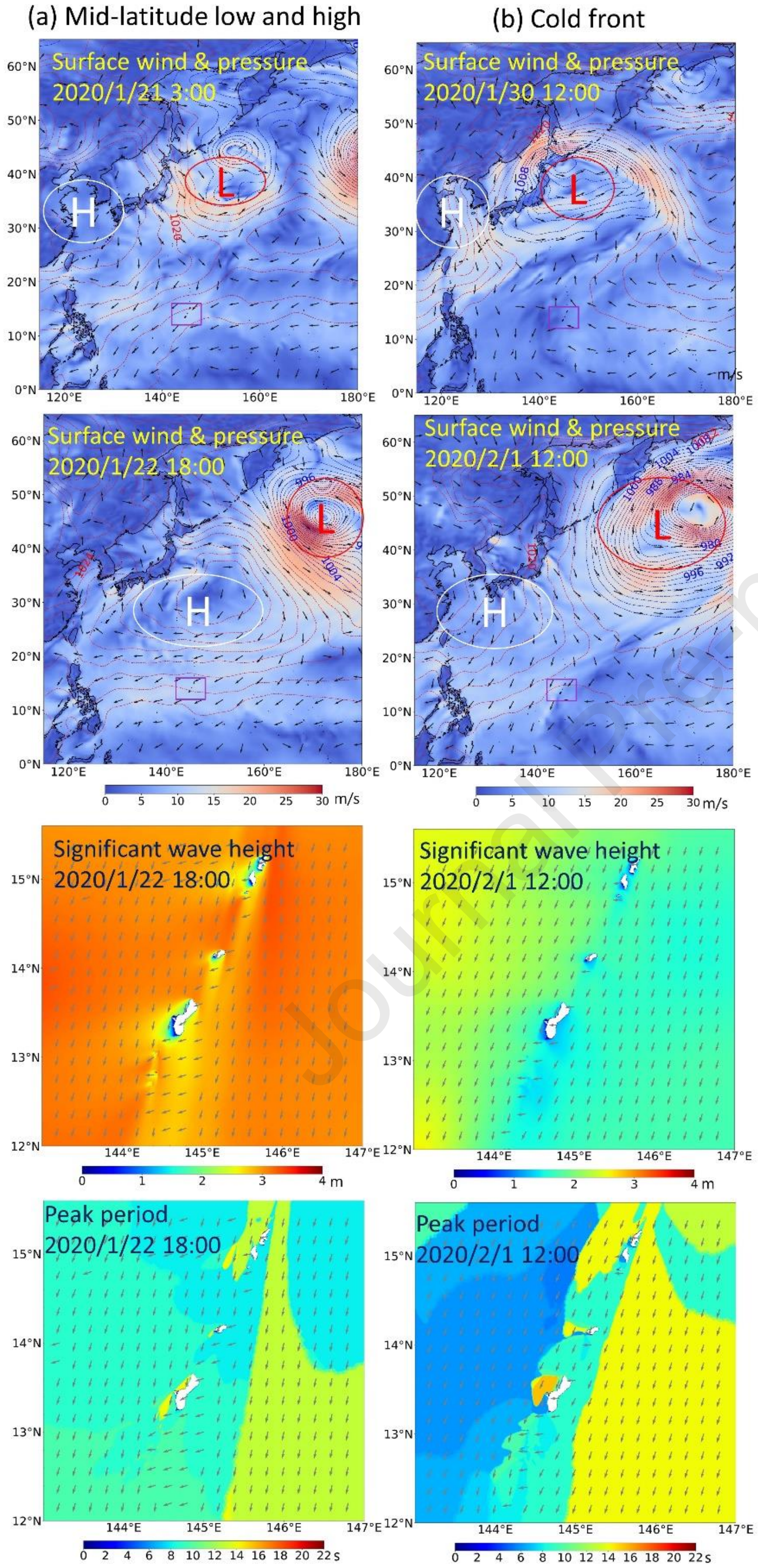

Figure 10. Representative winter weather systems in the Western and Central Pacific and wave patterns near Guam and the CNMI. (a) Mid-latitude low and high (b) Cold front

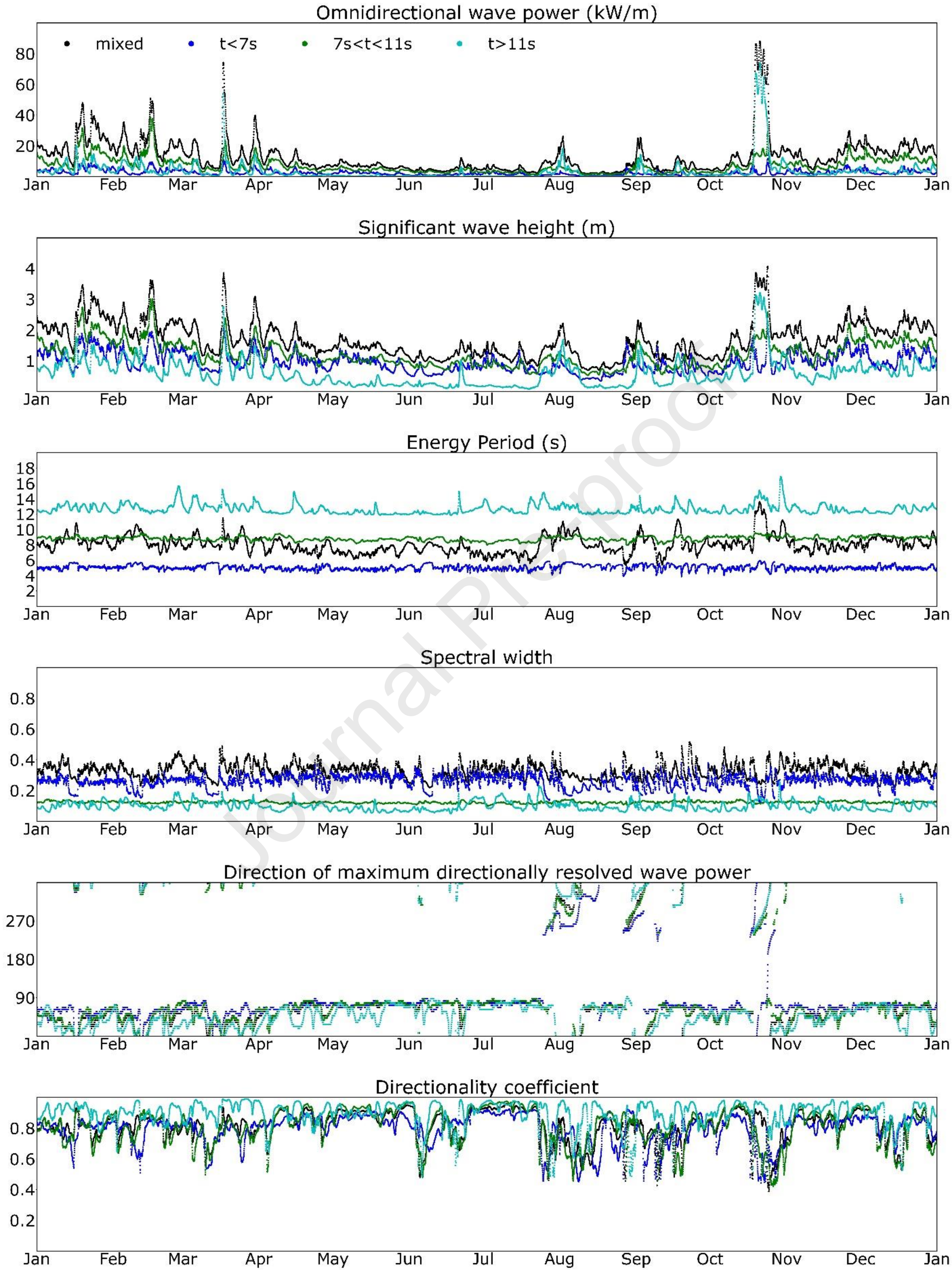

Figure 11. Time series of the six IEC wave energy resources parameters for the full and partitioned spectra from the hindcast at buoy #196 in 2017.

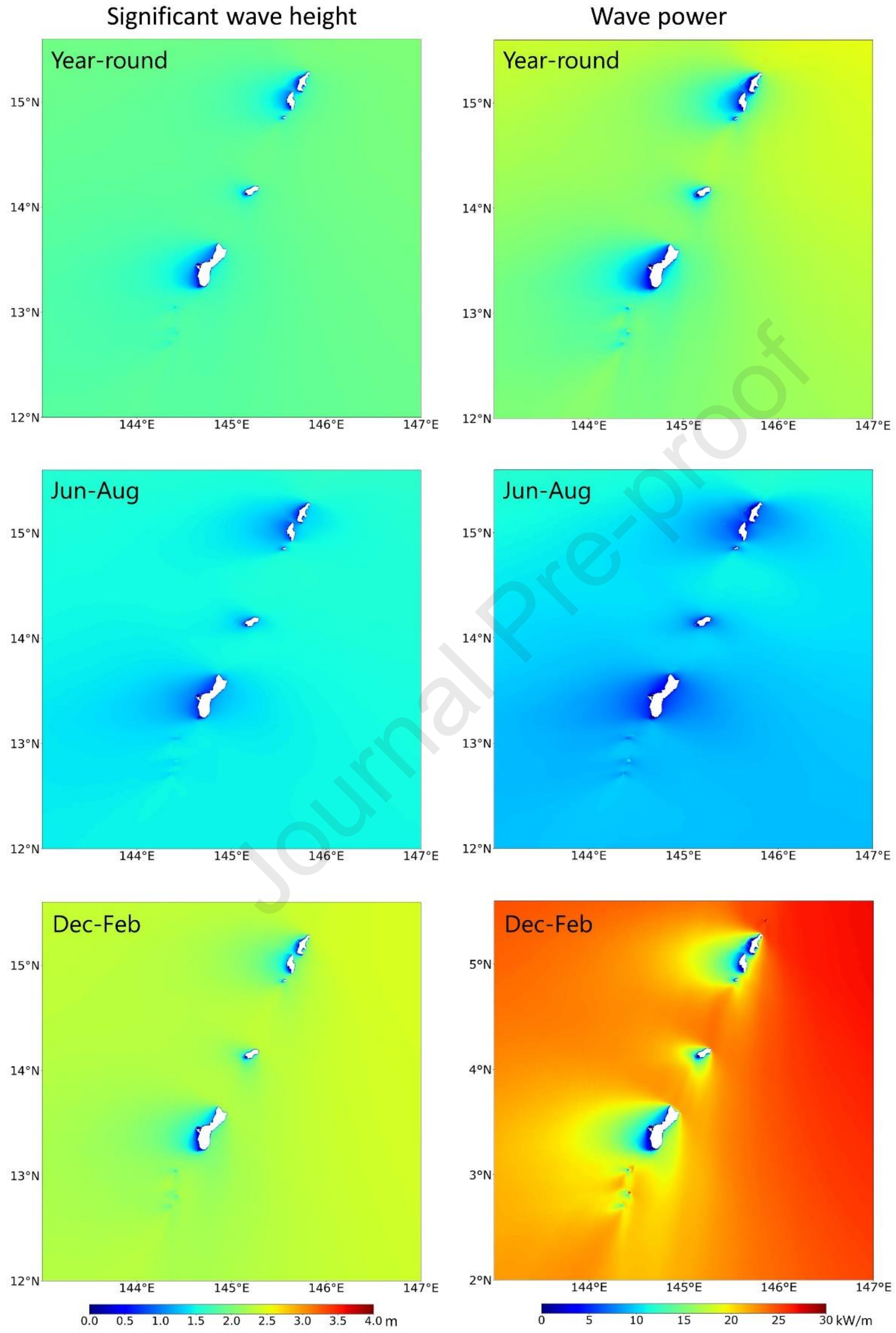

Figure 12. Year-round and seasonal averaged significant wave height and wave power from the 1979-2020 hindcast.

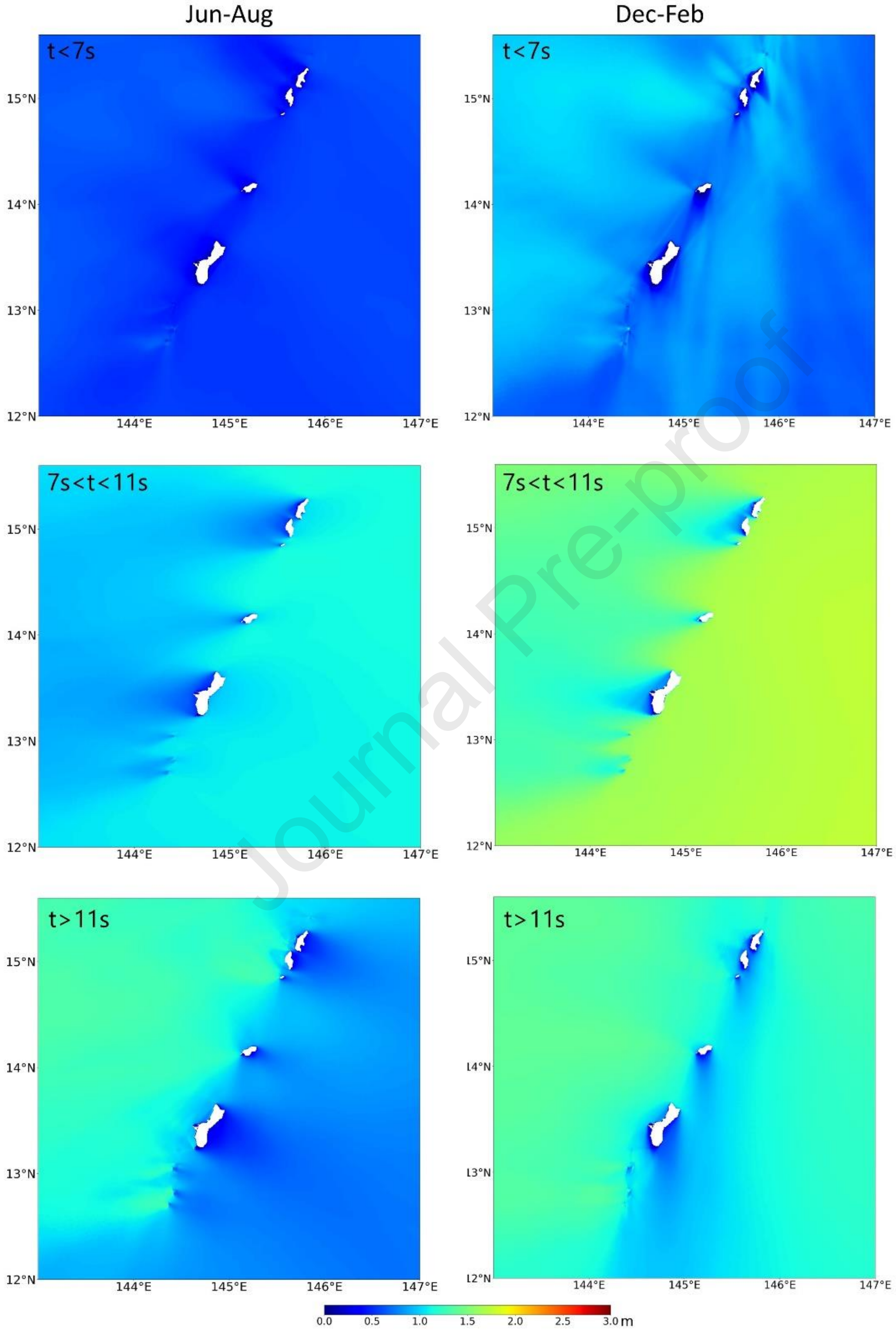

Figure 13. Seasonal average wave heights for spectral partitions of wind seas, wind waves, and swells from the 1979-2020 hindcast.

Appendix

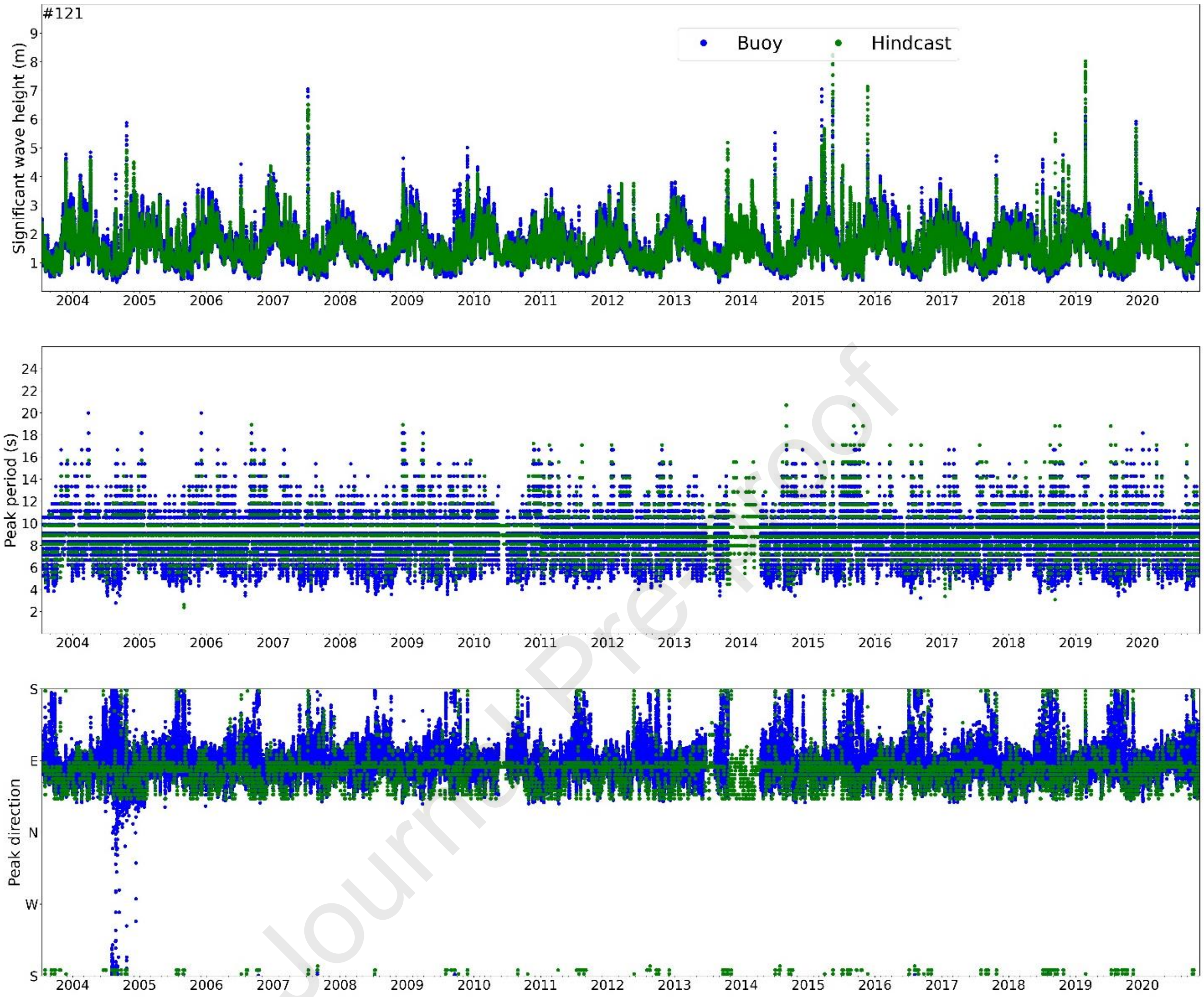

Figure A1. Time series of significant wave height, peak period, and direction from buoy #121 and the wave hindcast.

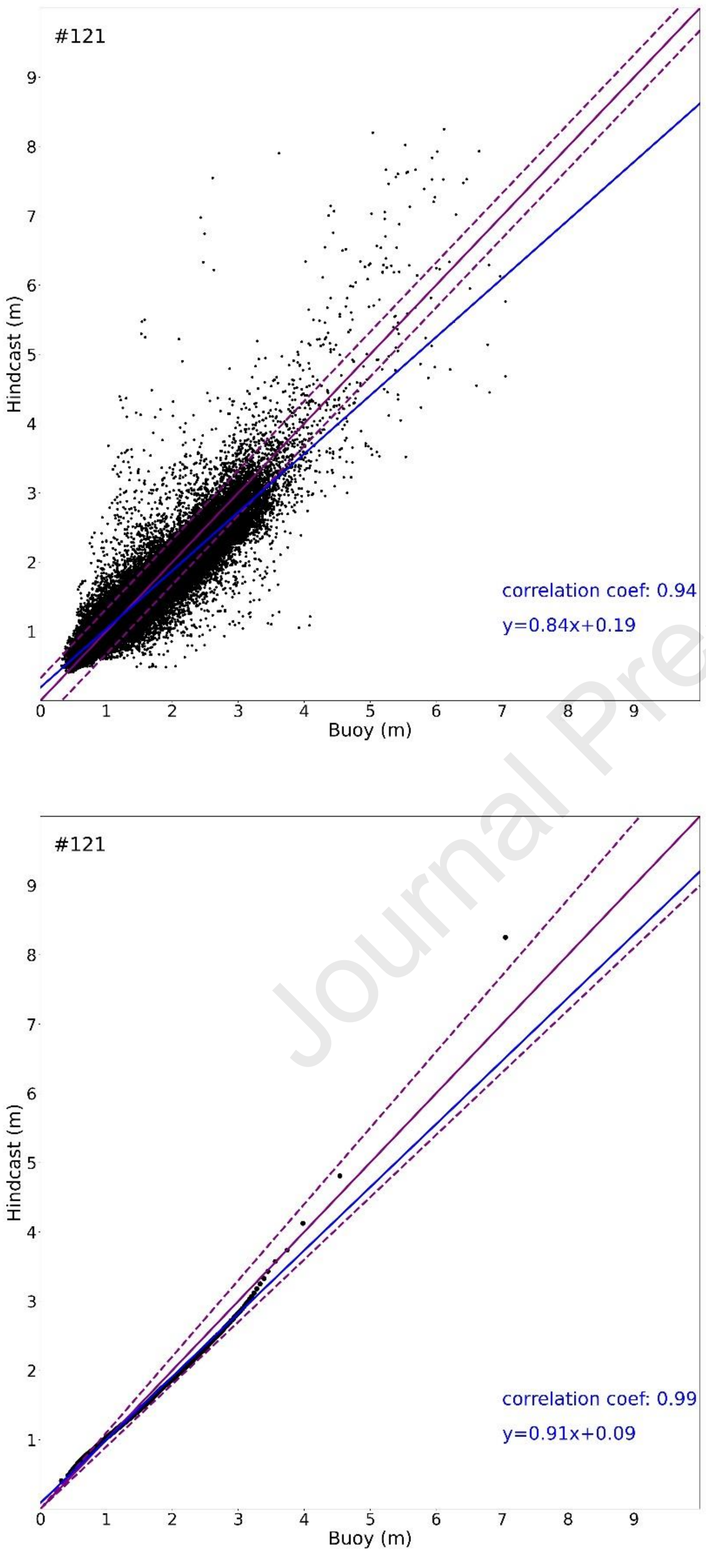

Figure A2. Scatter and Q-Q plots of measured and hindcast significant wave height at buoy #121.

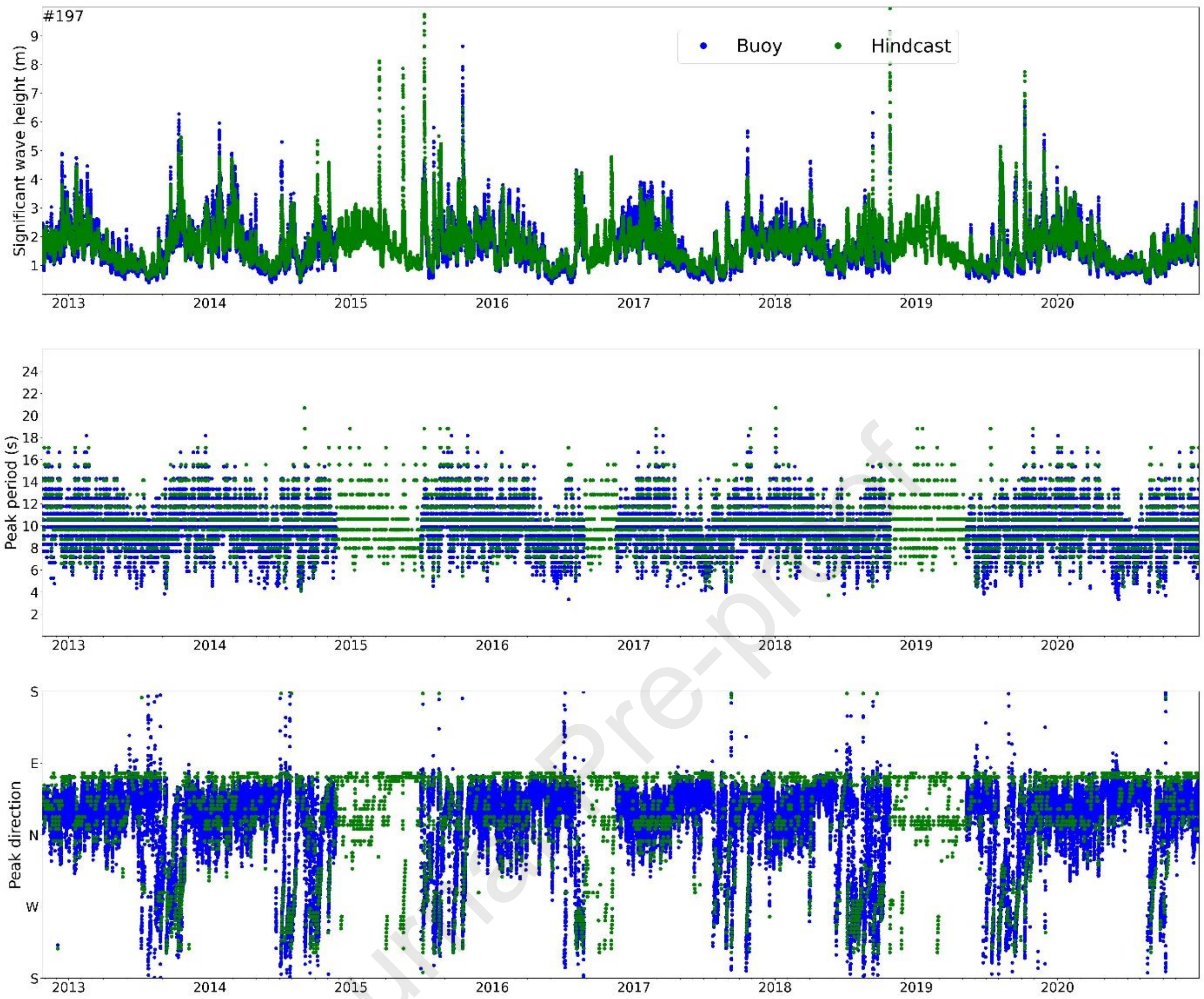

Figure A3. Time series of significant wave height, peak period, and direction from buoy #197 and the wave hindcast.

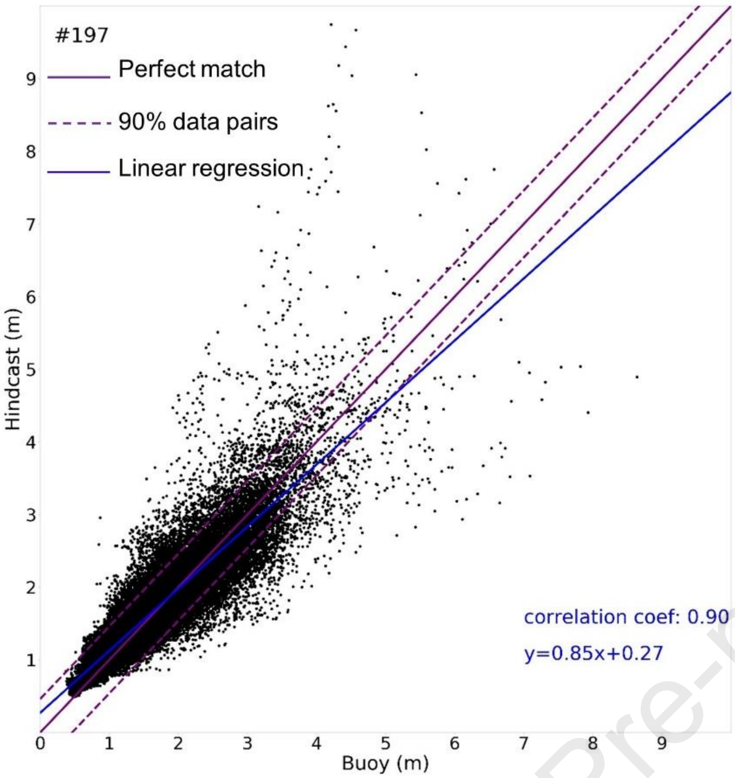

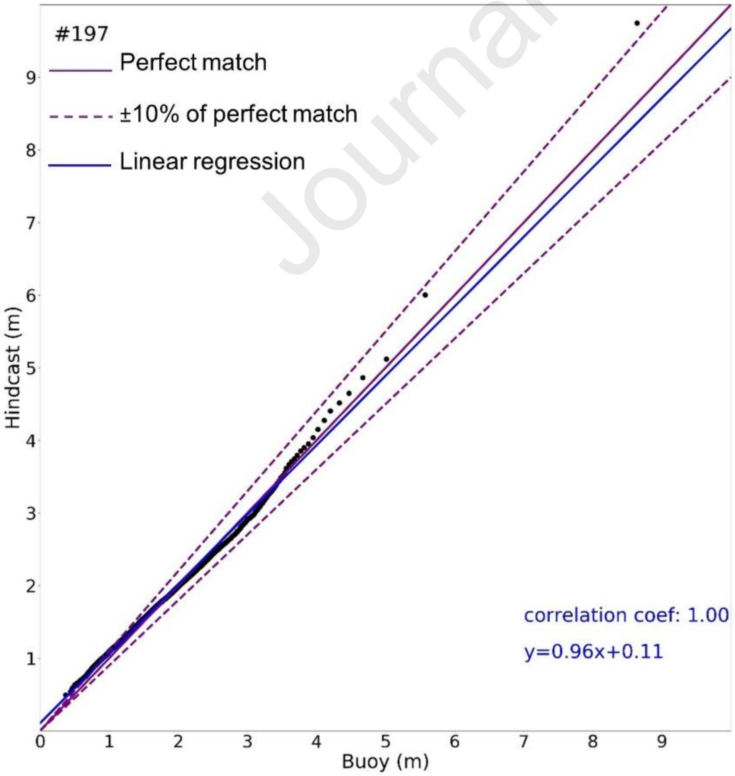

Figure A4. Scatter and Q-Q plots of measured and hindcast significant wave height at buoy #197.

Highlights:

- A 42-year wave hindcast by unstructured SWAN following IEC-TC 114 technical specifications.
- Hindcast validation of bulk and partitioned spectral energy for multimodal seas.
- Strong correlation between wave components to local and regional weather systems.
- Spatiotemporal descriptions of dominant wave components and energy levels.

Declaration of interests

☒ The authors declare that they have no known competing financial interests or personal relationships that could have appeared to influence the work reported in this paper.

☐ The authors declare the following financial interests/personal relationships which may be considered as potential competing interests: